TGF-β-induced DACT1 Biomolecular Condensates Repress Wnt Signaling To Promote Bone Metastasis

Mark Esposito[1], **Cao Fang**[1,*], **Katelyn C. Cook**[1,*], **Nana Park**[1], **Yong Wei**[1], **Chiara Spadazzi**[2], **Dan Bracha**[3], **Ramesh T. Gunaratna**[1], **Gary Laevsky**[1], **Christina J. DeCoste**[1], **Hannah Slabodkin**[1], **Clifford P. Brangwynne**[3,4], **Ileana M. Cristea**[1], **Yibin Kang**[1,5,6,#]

[1]Department of Molecular Biology, Princeton University, Princeton, NJ 08544, USA

[2]Osteoncology and Rare Tumors Center, Istituto Scientifico Romagnolo per lo Studio e la Cura dei Tumori (IRST) IRCCS, Meldola, Italy

[3]Department of Chemical and Biological Engineering, Princeton University, Princeton, NJ 08544,USA

[4]Howard Hughes Medical Institution, Princeton University, Princeton, NJ 08544, USA

[5]Ludwig Institute for Cancer Research, Princeton University, Princeton, NJ 08544, USA

[6]Cancer Metabolism and Growth Program, Rutgers Cancer Institute of New Jersey, New Brunswick, NJ 08903, USA

Abstract

The complexity of intracellular signaling requires both a diversity of molecular players and the sequestration of activity to unique compartments within the cell. Recent findings on the role of liquid-liquid phase separation provide a distinct mechanism for spatial segregation of proteins to regulate signaling pathway crosstalk. Here we discover that DACT1 is induced by TGF-β and forms protein condensates in the cytoplasm to repress Wnt signaling. These condensates do not localize to any known organelles but rather exist as phase-separated proteinaceous cytoplasmic bodies. Deletion of intrinsically disordered domains within the DACT1 protein eliminates its ability to both form protein condensates and suppress Wnt signaling. Isolation and mass spectrometry analysis of these particles revealed a complex of protein machinery that sequesters Casein Kinase 2, a Wnt pathway activator. We further demonstrate that DACT1 condensates are maintained *in vivo* and that DACT1 is critical to breast and prostate cancer bone metastasis.

[#]**Correspondence to:** Yibin Kang, Ph.D., Department of Molecular Biology, LTL255, Washington Road, Princeton University, Princeton, NJ 08544, USA, Phone: 609-258-8834, Fax: 609-258-2340, ykang@princeton.edu.
[*]Authors contributed equally

Keywords

Phase separation; biomolecular condensates; Wnt; TGF-β; DACT1; bone metastasis; breast cancer; liquid-liquid phase separation

Introduction

Interaction between the Wnt and TGF-β/Smad pathways plays a central role across different aspects of eukaryotic biology. The intersection of Wnt and TGF-β/SMAD signaling is required for a myriad of developmental events such as specifying the anterior-posterior axis or forming Spemann's organizer[1]. In adult physiology, opposing signaling by Wnt and TGF-β balances bone genesis and resorption[2, 3], and Wnt signaling drives colorectal cancer progression that is suppressed by TGF-β/SMAD4 signaling[4]. Despite numerous scenarios in biology where these pathways exert opposing or synergistic signaling, few nodes of positive or negative crosstalk between Wnt and TGF-β-SMAD are characterized.

A key site of Wnt and TGF-β coregulation is the bone, both in normal physiology and disease. For example, TGF-β–stimulated paracrine secretion of the Wnt inhibitors DKK1 or Sclerostin is essential for osteoclastogenesis[5, 6]. In parallel, Wnt-induced secretion of WISP1 attenuates SMAD2 phosphorylation to control osteoblast function[7]. In bone metastasis, TGF-β signaling sustains dormancy of disseminated tumor cells (DTCs) in bone[8] or osteolytic outgrowth through *PTHrP* and *Jagged1* induction[9–14]. Wnt signaling plays a dichotomous role in bone metastasis; Wnt inhibition by DKK1 is critical for immune avoidance by dormant micrometastases[15] and late-stage osteoclastogenesis[10, 16, 17]. On the other hand, engagement of bone vascular E-selectin by DTCs promotes metastatic colonization by activating Wnt signaling[18]. These findings imply a complex interplay between TGF-β and Wnt signaling in different stages of bone metastasis that allows efficient colonization, dormancy, and outgrowth.

In these jointly regulated processes, multiple layers of regulation between Wnt and TGF-β may exist beyond autocrine and paracrine signaling, such as intracellular phase separation. For instance, recent studies describe a membrane-less biomolecular condensate that discretely tunes the Wnt response via the destruction complex[19, 20]. Whereas these membrane-less organelles have only recently been described, with studies thus far focused on p-bodies and stress granules as the major types of cytoplasmic condensates[21–23], it is likely that this mechanism is broadly important to intracellular signaling.

To identify potential nodes of pathway crosstalk, we examined models of bone metastasis wherein cells discretely regulate Wnt and TGF-β signaling[15, 18]. This analysis identified DACT1 as a bone metastasis-promoting protein that functions as a cytoplasmic TGF-β-induced repressor of Wnt signaling through formation of organelle-like biomolecular condensates via multivalent interactions between intrinsically disordered domains. Isolation of these phase-separated organelles revealed a complex composition of protein machinery that sequestered Casein Kinase 2 (CK2), a kinase involved in the activation of Wnt signaling. These findings reveal a functional role for phase separation in the control of signaling dynamics in cancer.

Results

TGF-β transcriptionally induces DACT1 to repress Wnt activation

A powerful method to identify physiologically relevant signaling pathways in cancer metastasis is the selection of metastatic variants from parental cell lines via successive *in vivo* passaging followed by genetic profiling[24, 25]. We therefore derived a series of five sublines with various degrees of metastatic ability from the parental, weakly tumorigenic SUM159 triple negative breast cancer cell line through successive passaging *in vivo*[18, 26] (Extended Data Fig. 1a). All sublines established orthotopic tumors at a much greater rate than the parental line and acquired the ability to develop spontaneous lung metastasis (Extended Data Fig. 1b, c, e, f). However, only the SUM159-M1a derivative could efficiently develop spontaneous bone metastases (Extended Data Fig. 1d–f). Intracardiac injection of each subline confirmed that M1a was most proficient at forming metastatic lesions in bone (Extended Data Fig. 1g–i). This M1a derivative has been used in our previous studies of mechanisms of osteolytic metastasis[18, 27, 28]. Microarray followed by gene set enrichment analysis (GSEA) demonstrated that TGF-β signaling is the most enriched Hallmark signaling program in the M1a bone metastatic derivative compared to the parental SUM159 and was highly enriched compared to the closely-related but weakly bone metastatic subline M1L1 (Fig. 1a, Supplementary Table 1). The enrichment in TGF-β signaling in highly bone metastatic cells is corroborated by a similar analysis of the bone metastatic variants from the MDA-MB-231 triple negative breast cancer line[13, 25], underscoring the prominent role of this pathway in driving the development of bone metastasis.

We next assessed what specific genetic elements were associated with this increased bone metastatic potential and TGF-β signaling enrichment. Filtering and ranking of differentially expressed genes in highly bone metastatic M1a compared to the closely related but weakly metastatic SUM159 or M1L1 revealed 11 genes up-regulated by more than 4-fold (Extended Data Fig. 1j–k). To determine which of these 11 enriched genes were directly regulated by TGF-β, we cross-referenced this list first to ChIP-Seq data of SMAD2/3 binding elements[29] and then to a panel of genes induced by TGF-β at 3h in HaCaT, HPL1, MCF10A, and MDA-MB-231 cells[30, 31]. Only *Dishevelled binding antagonist of β-catenin 1 (DACT1, Dapper1, Frodo)* was present in each dataset, suggesting it as a candidate TGF-β downstream gene with potential bone metastasis-promoting functions. qRT-PCR analysis verified that *DACT1* was expressed at higher levels in M1a compared to other derivatives or parental SUM159 (Extended Data Fig. 1l). Addition of recombinant TGF-β to a panel of both normal and cancer lines followed by qRT-PCR at 3 and 12 hours showed that *DACT1* was strongly induced by TGF-β in all TGF-β-responsive but not SMAD4-deficient cell lines (Fig. 1b). These data demonstrate that TGF-β transcriptionally induces *DACT1*.

DACT1 is a cytoplasmic protein discovered in 2002 as a negative regulator of Wnt signaling via the stabilization of the destruction complex[32]. Developmental studies have since shown that DACT1 instead may activate Wnt signaling[33, 34], while other studies suggest that DACT1 alternately suppresses or activates Wnt depending on its concentration[35]. Mechanistically, the function of DACT1 has been attributed to diverse interactions, such as

with p120[36], Dishevelled[37], LEF[38], 14–3-3β[39], Vps34[40] or Miz1[41]; however, considerable uncertainty remains regarding how these interactions mediate the function of DACT1 or the directionality that they influence Wnt signaling. An exhaustive immunopurification assessment of DACT1 binding partners revealed that it indeed interacted with some of these previously described partner proteins as well as additional unknown interactions[42].

To measure if DACT1 impacts canonical Wnt signaling, we stably transduced both normal and cancer cell lines with lentiviruses expressing either a luciferase or GFP reporter driven by upstream TCF binding elements (12x-TCF-ffLUC or 7TGC)[18, 43, 44]. Validation of the Wnt reporters showed a marked increase of reporter activity following treatment with L cell-derived Wnt3a that was lost upon concurrent treatment with ICG-001, a specific inhibitor of canonical Wnt signaling (Extended Data Fig. 1m–n). Next, the reporter-labeled bone metastatic BM2 subline of MDA-MB-231[24, 25] or normal human pulmonary epithelial cells HPL1 were stably transduced with DACT1 shRNA, shControl (scrambled control shRNA), empty vector, or a human DACT1 overexpression cassette. Subsequent *DACT1* knockdown or overexpression levels were then confirmed by qRT-PCR (Extended Data Fig. 2a–b). Treatment with Wnt3a for 20 hours followed by assessment of luciferase activity revealed that *DACT1* knockdown (KD) more than doubled Wnt reporter activation by Wnt3a while *DACT1* overexpression moderately reduced Wnt3a-dependent reporter activity (Fig. 1c). Analysis of 7xTCF-GFP reporter activity on a cell-by-cell basis via flow cytometry similarly revealed that *DACT1* KD increased Wnt3a-induced GFP expression while *DACT1* overexpression reduced GFP signal in both BM2 and HPL1 cells (Extended Data Fig. 2c–d).

Orthogonal techniques further validated the suppression of Wnt signaling by DACT1 as *DACT1* knockdown increased β-catenin nuclear localization in the Wnt3a-induced state (Fig. 1d, Extended Data Fig. 2e). *DACT1* knockdown further increased total β-catenin protein in Wnt3a-treated cells (Extended Data Fig. 2f). This increase in β-catenin was not accompanied by changes in DVL2 or DVL3 levels in any of the DACT1-modified cell lines (Extended Data Fig. 2f), suggesting that DACT1 does not promote degradation of Disheveled to increase β-catenin destruction in this model system, which contrasts to prior studies[37]. Analysis of β-catenin expression in normal epithelial HPL1 cells also demonstrated that *DACT1* levels inversely correlated to β-catenin levels upon Wnt3a stimulation (Extended Data Fig. 3a). Finally, qRT-PCR analysis of the Wnt downstream gene *AXIN2* revealed higher induction at 24 and 48h in *DACT1* KD cells compared to the control cells (Extended Data Fig. 3b). Collectively, these data suggest that DACT1 negatively regulates canonical Wnt signaling.

We therefore hypothesized that TGF-β induces *DACT1* to negatively regulate Wnt signaling. To test this, we assessed the effects of TGF-β and LY2109761, a selective TGF-βRI/II receptor inhibitor, on Wnt signaling in M1a-7TGC and BM2–7TGC cell lines. We reasoned that since the M1a line shows enriched TGF-β signaling (Fig. 1a), treatment with a TGF-β inhibitor should enhance Wnt signaling by preventing TGF-β-induced *DACT1* expression. Flow cytometry of M1a-7TGC cells pre-incubated for 24 h with LY2109761 or TGF-β followed by 24h of Wnt3a stimulation demonstrated that TGF-β treatment indeed suppressed the already low levels of Wnt activation while LY2109761 increased Wnt activation (Fig. 1e). Testing in the BM2–7TGC line confirmed that exogenous TGF-β

addition attenuated Wnt3a-mediated Wnt activation (Extended Data Fig. 3c). We next showed that these results were dependent on DACT1 as knockdown in the BM2 line reduced the magnitude of TGF-β-mediated suppression of Wnt signaling compared to control while DACT1 overexpression enhanced this effect (Extended Data Fig. 3d–e).

DACT1 forms biomolecular condensates driven by intrinsically disordered domains

As the data showed DACT1 does not affect Dishevelled stability whereas it does influence β-catenin protein levels, we next sought to determine the mechanism by which DACT1 regulates Wnt signaling. Multiple molecular interactions in different cellular compartments have been ascribed to DACT1[37, 45]; these include reports that DACT1 shuttles between the nucleus and cytoplasm to prevent β-catenin binding to TCF/LEF transcription factors[38], or interacts with Vps34 to initiate the autophagosome[40].

To test the localization of DACT1, we generated TdTomato N-terminal and C-terminal fusions to DACT1 that were expressed in both M1a and BM2 cells while TdTomato-only was expressed as a control. Stable expression of either the N-terminal or C-terminal fusion proteins in either cell line revealed a unique punctate localization of TdTomato-positive DACT1 bodies (1–5 bodies per M1a cell and 1–20 bodies per BM2 cell), each of which ranged in size from <200 nm to 2 μm. This result was not observed in TdTomato-only cells (Fig. 2a). The localization of these bodies was not affected by 12h Wnt3a treatment (Extended Data Fig. 4a.), while the same puncta were also observed in the HPL1 normal epithelial cell line (Extended Data Fig. 4b). Both DACT1-TdTomato fusion proteins as well as native DACT1 protein were actively degraded as shown by cycloheximide pulse-chase (Extended Data Fig. 4c). This degradation was mediated by the ubiquitin-proteasome system and not the lysosomal system as demonstrated by treatment with either MG-132 or Bafilomycin A, which are inhibitors of the respective protein degradation pathways (Extended Data Fig. 4d). Staining for a panel of organelle markers revealed that these DACT1-containing organelle-like structures did not co-localize with mitochondria, p-bodies, endosomes, lysosomes, autophagosomes, the ER or the Golgi apparatus (Extended Data Fig. 4e). To verify that DACT1 bodies are not caused by fusion to TdTomato, we stained for endogenous DACT1 protein and found the same structures were formed in native cells (vector control in Extended Data Fig. 5a) and cells expressing either wild-type *DACT1* or DACT1-TdTomato; notably, the DACT1 puncta were absent in DACT1-knockdown cells (Extended Data Fig. 5a–b). Importantly, both the N-terminal and C-terminal DACT1-TdTomato fusions could efficiently repress Wnt reporter activation compared to TdTomato alone (Fig. 2b), indicating that both fusions preserved the Wnt-suppressive function of DACT1.

Given that these DACT1 bodies did not co-localize with other organelles, including autophagosomes, did not show nuclear localization, and that they exhibited Wnt suppressive function, we next sought to understand what these structures were. SoRa super-resolution imaging of 293-T cells transfected with DACT1-TdTomato revealed an assortment of structures that were mostly spherical, yet some of which were tubular or hollow (Extended Data Video 1). Further interrogation using holotomographic-fluorescent imaging co-localized TdTomato signal with cell-wide measurement of the refractive index. Analysis of

these images in both M1a and BM2 cells revealed perfect co-localization of TdTomato signal with distinct regions of locally increased refractive indices (Fig. 2c, Extended Data Fig. 5c). Computational sectioning of the images revealed red-fluorescent areas mapped to refractive indices between 1.36–1.38, a value normally observed for condensed protein assemblies (Fig. 2d)[46].

Intracellular protein condensates provide a distinct mechanism for spatially restricted zones of signaling as compared to lipid membrane segregation[47, 48]. Additionally, components of the Wnt signaling pathway, including AXIN1 and APC, have been recently shown to associate together in phase separated condensates critical for activity of the β-catenin destruction complex[49]. Co-transfection of AXIN1-GFP and DACT1-TdTomato into 293T cells revealed that both proteins formed condensates; however, these formed into distinct structures (Fig. 2e). Live imaging studies of DACT1-TdTomato fusions in cells showed both Brownian and directed movement of these bodies with fusion events occurring between them (Supplementary Video 2). Fluorescence recovery after photobleaching (FRAP) further supported that these were dynamic assemblies; partial recovery of fluorescence (Fig. 2f, Supplementary Video 3–4) showed both immobile and mobile populations are present, similar to other condensates[50, 51].

Liquid-liquid phase separation of proteins is driven in many cases by intrinsically disordered domains (IDRs)[21]. Prediction of DACT1 IDRs using D^2P^2 identified 10 disordered regions that we deleted from the DACT1-TdTomato sequence in addition to the previously reported PDZ, coiled-coil, nuclear export and nuclear localization domains of DACT1 (Extended Data Fig. 6a, Supplementary Table 2). Stable generation of each DACT1-TdTomato variant was confirmed by western blot (Fig. 3a, note that DR7 contains the antibody recognition epitope and therefore escaped western blot detection). Fluorescence imaging demonstrated that only two of the IDR deletions (DR7 and DR8) affected the formation of intracellular condensates (Fig. 3b). Meanwhile, deletion of the reported NES and NLS sites had no effect on formation of condensates or their localization, whereas deletion of the coiled-coil domain led to a loss of expression (Fig. 3a–b).

We next tested the functional impact of IDR deletions on DACT1-mediated Wnt suppression by introducing each mutant into BM2–7TGC cells. Wnt3 activation revealed that only mutations DACT1 DR7 and DACT1 DR8, which disrupted the formation of protein condensates, and mutations DACT1 DR1 and DACT1 coiled-coil, which reduced DACT1 protein expression (Fig. 3a–b), alleviated DACT1-mediated Wnt repression (non-significance compared to the upper threshold set by TdTomato-only and significance comparing to DACT1 wild-type as the lower threshold). Other deletions led to either a null effect or a gradient of responses (Fig. 3c). One exception to this trend was DACT1 NES, which did not reduce DACT1 expression but is contained within the coiled-coil domain and whose deletion led to a loss of DACT1 activity. Notably, DR7 and DR8 represent larger deletions (Supplementary Table 2) and correspond well with the length of fragments observed in the Fus protein to be sufficient for phase separation[52]. Next, we tested the sufficiency of either DR7 or DR8 to phase separate without the remainder of the DACT1 protein. Both fragments were tagged with TdTomato and stably expressed in M1a and BM2 cells. While DR7 was insufficient to force phase separation in either M1a or BM2 cells, DR8

was sufficient to form large punctate bodies in the nucleus of either cell line (Extended Data Fig. 6b–c). The altered localization of DR8 condensates was likely driven by the NLS domain found within this fragment (Extended Data Fig. 6a).

These data suggest that DACT1 phase separation is the actuating mechanism of Wnt suppression. We therefore sought to directly test this via two methods: We introduced DACT1-TdTomato into 7xTCF-GFP-SV40-puromycin reporter cells and stimulated with Wnt3a for 24h. Live imaging revealed that longer Wnt3a stimulation (24h-30h) led to diffusion of DACT1 from a punctate to a diffuse localization that presented heterogeneously across cells within the same cell dish. We observed a tight correlation between those cells with diffuse DACT1 and active Wnt signaling as measured by GFP. Meanwhile, those cells that maintained DACT1 condensates were not Wnt positive (Fig. 3d, upper panel). In parallel, DR7 deletions showed exclusive diffuse cytoplasmic localization and were uniformly GFP positive (Fig. 3d, lower panel). Next, we introduced an amino acid sequence from the Fus protein known to promote phase separation[52] in place of the DR8 sequence. This DACT1 hybrid sequence could form punctate bodies and suppressed Wnt activation compared to the DACT1 DR8 mutant alone (Fig. 3e–f). Importantly, these effects were lost when a mutant Fus residue with 27 separate Y > S substitutions was used as a negative control[52] (Fig. 3e–f). These data indicate that rescue of phase separation of DACT1 protein segments outside the DR8 region is at least partially sufficient for supporting the Wnt-repressive functions of DACT1.

DACT1 biomolecular condensates contain RNA-binding, translational and signaling protein components

Data presented here show that phase separation is the central characteristic driving DACT1 function in both cancerous and normal cells. However, this is not mutually exclusive of its other reported roles as it may sequester important Wnt pathway components to modify Wnt signaling. Indeed, immunopurification studies have demonstrated that DACT1 binds a variety of proteins, including itself, Dishevelled, β-catenin, VPS34, DACT2, DACT3 etc.[42]. Meanwhile, prior characterization of cytoplasmic condensates have focused on p-bodies and stress granules which are hybrid protein-RNA condensates[48]. Therefore, we tested whether these DACT1 particles contain *β-catenin* mRNA to prevent translation as our data showed that DACT1 levels inversely correlate with β-catenin protein level in the Wnt-activated state (Extended Data Fig. 2f). Fluorescent *in situ* hybridization revealed that DACT1 condensates did not bind *β-catenin* mRNA (Extended Data Fig. 6d).

To investigate the protein contents of these DACT1 condensates, we developed a method to separate them intact from cells. We found that multiple methods of conventional lysis as well as prior methods used to isolate p-bodies[53] led to the formation of non-specific aggregates in DACT1-TdTomato, TdTomato, and DACT1 DR7-TdTomato mutants. Rather, we found that low amplitude sonication followed by the addition of 1% Triton X-100, 0.5% Sodium Deoxycholate, RNAse inhibitors and Hoechst 33342 yielded excellent separation of DACT1-TdTomato-positive, Hoechst-negative particles in control or Wnt3a stimulated cells, but did not identify particles in the TdTomato or DACT1 DR7-TdTomato mutant cells (Fig. 4a).

We next employed fluorescence-activated particle sorting to isolate these particles and analyzed their composition with liquid chromatography tandem mass spectrometry (LC-MS/MS), quantifying the DACT1-particulate proteome in both control and Wnt3a-stimulated conditions (Extended Data Fig. 7a). Following stringent data quality filtering and analysis, we found DACT1 to be the most abundant protein in the isolated particles, which contained approximately six hundred other proteins (Supplementary Table 3). Additional analysis of the mass spectrometry data uncovered a striking enrichment in proteins involved in RNA processing, ribosome assembly, translational control, and protein folding (Extended Data Fig. 7b–c, Supplementary Table 4). This included many members of the spliceosome (*e.g.*, SNRPs, GEMIN7, TRA2A/B, ribosome assembly factors (*e.g.*, RPF2, PES1, NIP7), the large and small ribosomal subunits, translation initiation factors (*e.g.* EIF6), and protein-folding chaperones (*e.g.*, HSPA1a, BAG2), among others. The particle proteome also contained proteins that control cellular organization and trafficking, such as actin-nucleating and regulating proteins (*e.g.*, CAPs, ARPC1b), supporting the dynamic behavior of DACT1 particles in cells.

We also observed that Wnt3a changed the abundance of the identified proteins between the control and Wnt3a conditions rather than composition (Fig. 4b). Across independent isolations, the control and Wnt3a conditions exhibited nearly complete consistency in terms of detected proteins (Fig. 4b, Supplementary Table 3). Instead, 26 proteins had more than 2-fold increases in the Wnt-treated condition and 11 proteins were decreased by more than 2-fold (Fig. 4b). These data suggest that Wnt3a stimulation does not change the proteins found within particles but rather alters the relative abundance of these proteins, perhaps reflecting the biological processes such as translational initiation or RNA-binding that may potentially be involved in these DACT1-dependent condensates (Extended Data Fig. 7c). The majority of phase separated condensates have been characterized as protein-RNA hybrids contained in p-bodies and stress granules[21, 31]; importantly, mass spectrometry did not identify either Fus or DCP1a (Supplementary Table 3), which are integral components of stress granules and p-bodies.

A key enriched candidate within this data was Casein Kinase 2, with all subunits, including α, α' and β, detected at high enrichment levels (Fig. 4b, Supplementary Table 3). CK2 is a well-known positive regulator of Wnt signaling[54], and has further been detected as a DACT1 binding partner by high-throughput yeast two-hybrid screens[55]. Indeed, immunostaining showed co-localization of CK2 to DACT1-TdTomato bodies (Fig. 4c), confirming that our isolation method identified *bona fide* DACT1 binding partners in cells. Treatment of BM2–7TGC lines with Silmitasertib, a specific CK2 inhibitor, confirmed that CK2 inhibition decreases Wnt activity (Fig. 4d). As expected, DACT1-overexpressing cells had lower basal Wnt activity, and were less sensitive to Silmitasertib-induced Wnt suppression than vector control cells (Fig. 4d, e).

This data suggests that DACT1 reduces the available pool of CK2 necessary to sustain maximal Wnt signaling, potentially through sequestration of CK2 into these biomolecular condensates (Fig. 4c). To test this hypothesis, we tethered CSKN2A1 (CK2α subunit) to GFP and expressed by itself or in tandem with DACT1-TdTomato in both M1a and BM2 cells. Confocal imaging revealed that CK2α diffusely localized to both the nucleus and

cytoplasm when expressed by itself, while coexpression with DACT1-TdTomato resulted in exclusive sequestration of the cytoplasmic pool to the condensates while the nuclear pool remained diffusely localized (Figure 5a, Extended Data Fig. 8a, Supplementary Video 5). Further testing of this finding by particle flow cytometry revealed that CK2α-GFP was found in all DACT1-TdTomato particles (Figure 5b, Extended Data Fig. 8b). This data demonstrated that DACT1 is dominant over cytoplasmic CK2 by sequestering CK2 to DACT1-generated phase separations. Importantly, DACT1-overexpressing cells were still partially sensitive to Silmitasertib, an observation that may be explained by the presence of CK2 localized to the nucleus that was not accessible to sequestration within the DACT1 particles (Fig. 4c–e).

DACT1 expression is critical for bone metastasis

Here we describe an unexpected function for DACT1, and, given that phase separation is a recently described phenomenon in cells, we were interested in understanding whether DACT1 condensates were indeed functional in a relevant *in vivo* context. As DACT1 expression was elevated in bone metastatic cells (Extended Data Fig. 1), we assessed the functional importance of DACT1 in breast and prostate cancer bone metastasis. We validated two shRNA constructs that reduced *DACT1* mRNA levels in the M1a derivative and that did not affect proliferation of the cells *in vitro* (Extended Data Fig. 9a–b). Injection of these cells via left ventricle in nu/nu female mice resulted in dramatically slower bone metastasis progression by bioluminescence and X-ray compared to control cells (Fig. 6a–d). This result was further confirmed in BM2 breast cancer cells (Extended Data Fig. 9c–g) and DU145-ob2b prostate cancer cells, a bone metastatic subline that we had derived from two successive isolation of bone metastatic cells *in vivo* after intracardiac injection of the parental DU145 cell line[18] (Extended Data Fig. 9h–i). Next, we assessed bone metastasis of M1a cells overexpressing either wild-type DACT1 or its ΔR7 and ΔR8 mutants. Ectopic expression of neither DACT1 nor ΔR8 significantly affected bone metastasis development, likely because sufficient level of endogenous DACT1 already expressed in these cells. However, overexpression of ΔR7 mutant suppressed metastasis (Extended Data Fig 9j–k), possibly due to a dominant negative effect of ΔR7 on wild-type DACT1, an observation supported by Wnt suppression data (Figure 3c). To assess if DACT1 formed biomolecular condensates in the *in vivo* setting, we injected DACT1-TdTomato expressing BM2 cells and imaged active bone metastases *ex vivo;* results demonstrated that cytoplasmic condensates also form in the *in vivo* context (Fig. 6e–f).

To test our findings in the clinical setting, we analyzed signaling programs correlated to *DACT1* expression. Analysis showed that the TGF-β signaling and the EMT gene sets were strongly enriched among genes correlated with *DACT1* in the METABRIC clinical dataset[56], suggesting DACT1 and its co-regulated genes are influenced by TGF-β signaling in human breast cancer (Extended Data Fig. 9l–m). To further assess the clinical relevance of DACT1, we analyzed the EMC-MSK breast cancer clinical dataset with annotations for organ-specific metastatic relapse[57]. Results indicated that higher *DACT1* expression is associated with a higher risk of developing bone metastasis, but is not linked to metastatic relapse to other organ sites such as the lung, liver, and brain (Fig. 6g, Supplementary Table 5).

Discussion

Here we describe the functional mechanism of DACT1 in the suppression of Wnt signaling through the generation of phase-separated biomolecular condensates. Previous studies of DACT1's function have not agreed on the directionality or the mechanism, yet have identified multiple binding partners such as Dishevelled, β-catenin, Vps34[45], and even itself, suggesting that a unified understanding of DACT1 was absent[42]. Here we show that DACT1 serves as a scaffold to generate phase-separated condensates and, by leveraging the ability of phase-separated granules to persist in cell-free systems[52, 53], we developed a robust method to reveal >600 protein constituents in these DACT1 condensates. A few of these constituents have been described by previous DACT1 binding screens, including HDAC1[38] or CK2[55]. Given the complexity of this DACT1-associated proteome, it is unlikely that Wnt suppression is the sole function of DACT1.

The identification of protein regulatory, RNA-binding, and translational machinery in these condensates is paralleled by prior descriptions of phase separation in which RNA-protein hybridization is the driving force behind the formation of these organelle-like structures[31]. Whereas our mass spectrometry data identified numerous RNA-binding proteins previously identified as putative components of other phase separated systems[31], we did not identify the essential stress granule or p-body proteins Fus or Dcp1a. In combination with immunostaining showing that these DACT1 particles do not co-localize with major organelles, p-bodies (Extended Data Fig. 4e) nor AXIN1-driven condensates (Fig. 2e), the data here support these DACT1 particles as organelle-like structure that serves as a central node to integrate TGF-β and Wnt signaling.

The field of phase separation and regulation of biomolecular condensates has received considerable attention as a distinct biophysical mechanism underlying spatial regulation[21, 31, 58]. This is particularly important to the interplay of Wnt and TGF-β signaling as few nodes of crosstalk have emerged between these pathways. The data here indicate that DACT1 condensates prevent Wnt signaling activation by interfering with CK2 activity; however, this is likely only one of its roles. Highlighting this, nonsense mutations in DACT1 Trp419, located in DR7, causes an autosomal dominant disorder with features overlapping Townes-Brock Syndrome[59].

These data, when combined with previous studies of bone metastasis, suggest a model wherein initial binding of bone metastatic cells to the sinusoidal vasculature temporarily induces Wnt signaling needed for the initial disseminated phase[18]. DACT1 is then induced by TGF-β, which is abundant in the bone matrix, to suppress Wnt signaling in the dormancy stage[15]. Further metastatic outgrowth in the bone then stimulates osteoclastogenesis, which further increases the local TGF-β concentration[9], leading to *DACT1* induction and subsequent Wnt suppression that has been shown to be important to the development of osteolytic macrometastases[16]. Despite strong evidence for this model from multiple distinct studies, future studies should assess the temporal contribution of DACT1 to bone metastatic progression. This study opens the door to future investigations into the biogenesis and function of the DACT1 particles across cellular biology in normal development and disease.
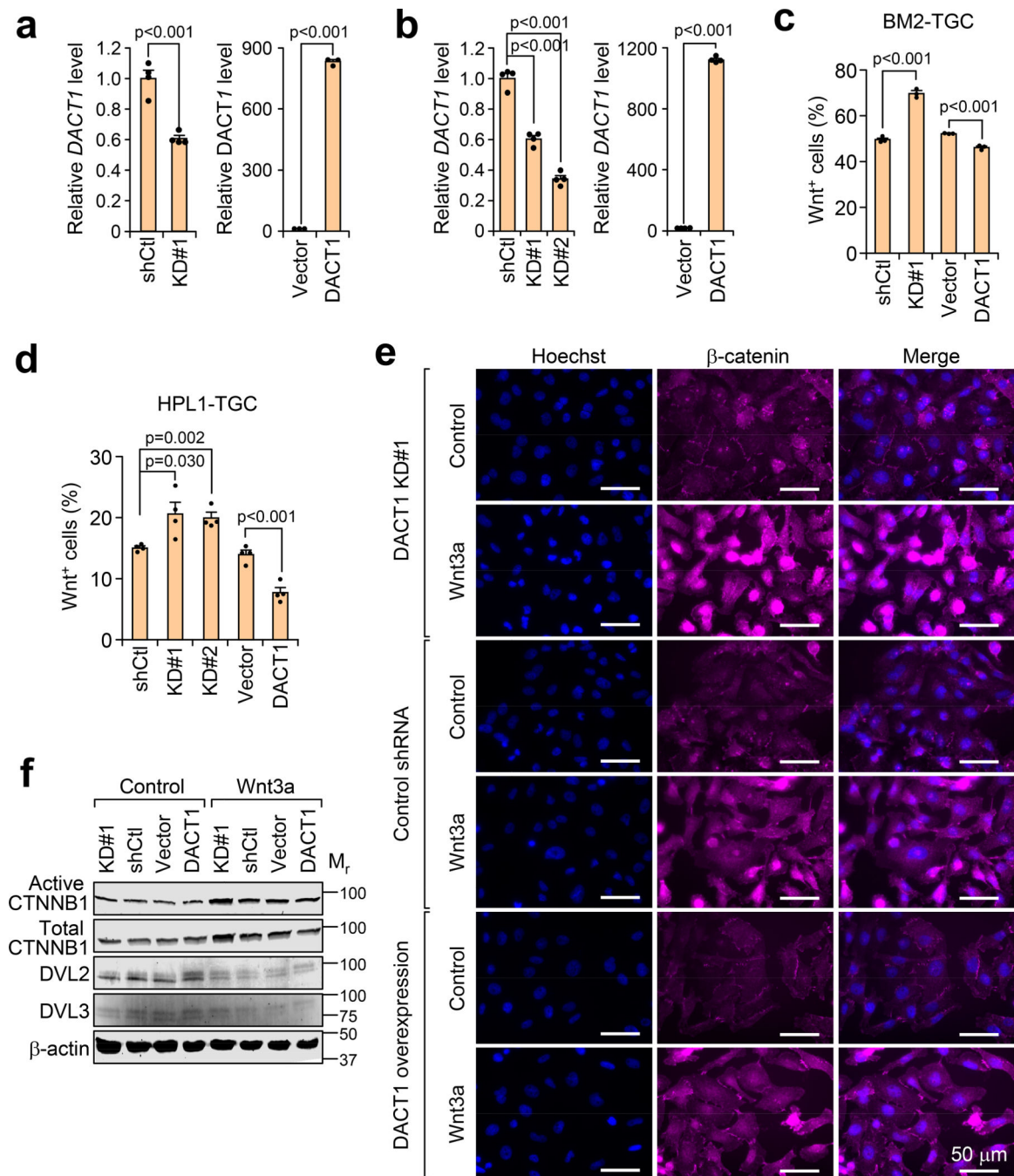
Extended Data
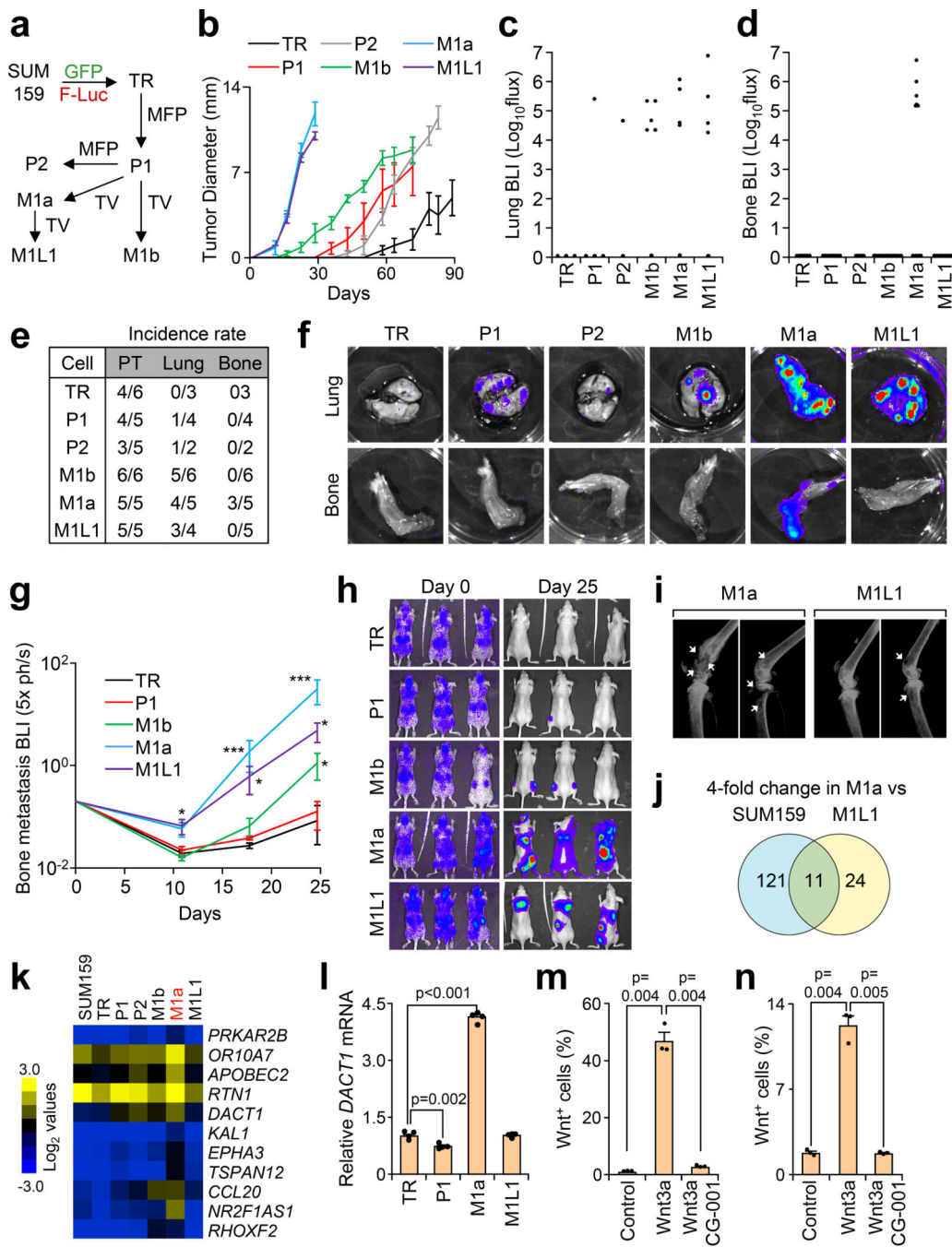
Extended Data Fig. 1. Characterization of the metastatic variants of SUM159 breast cancer cell line identifies *DACT1* as a highly expressed gene in the bone metastatic M1a subline.

a, Schematic summary of the establishment of a series of isogenic sublines with different primary tumor and metastasis potential from the parental SUM159 triple negative breast cancer cell line. Parental SUM159 cells were stably labeled with a retroviral triple reporter (TR) expressing GFP, thymidine kinase, and firefly luciferase (F-luc) and injected into the mammary fat pad of nude mice. A primary tumor was isolated, cultured, and re-injected by

either tail-vein or mammary fat pad injection. Successful outgrowths were then isolated and cultured. **b**, Isolated cell lines were injected orthotopically into NSG mice and monitored for primary tumor growth. n = 5 mice/group. Student's t-test. Representative of 2 independent experiments. **c**, **d**, **e**, *Ex vivo* imaging of bones and lungs was conducted once primary tumors reached mean diameter >1 cm. Values for lung (**c**) and bone (**d**) metastasis were thresholded to 0 at values below 10^4 and 10^5 photon/sec, respectively, to remove background noise. Individual hindlimbs were treated as independent data points. Rates of successful outgrowth were enumerated per group (**e**). **f**, Representative *ex vivo* bioluminescence images of spontaneous metastasis to lung and bone from each derived subline from (**c-e**). **g**, The development of bone metastasis after intracardiac injection of each derivative was monitored by bioluminescent imaging and was compared to SUM159-TR. Mann-Whitney U test. n = 6 mice/group. **h,i**, Representative bioluminescent (**h**) and X-ray images (**i**) at day 0 and day 25 of mice from (**g**). **j**, Gene expression values from microarray analysis were used to generate a list of genes up-regulated >4-fold in M1a compared to either SUM159PT-TR or M1L1. **k**, Heatmap representation of the expression levels of the 11 differentially expressed genes from (**j**). **l**, Quantitative real-time PCR (qRT-PCR) analysis of *DACT1* mRNA levels normalized to *Gapdh* in the indicated SUM159 sublines. n = 4 technical repeats, representative data from 2 independent experiments. **m**, **n**) Flow cytometry measurement of 7x-TCF-GFP Wnt reporter activity in BM2 (**m**) or HPL1 (**n**) cells with Wnt3a and Wnt inhibitor ICG-001 (25 μM) treatment. n = 3 biological replicates. Student's t-test. Experiment independently repeated 3 times. Data represents mean ± SEM. * p< 0.05, ** p<0.01, *** p<0.005 in **g** with exact p values in Source Data. Numerical source data for **b-e, g, l-n** are provided.

**Extended Data Fig. 2. DACT1 represses Wnt signaling.**

a,**b**, qPCR analysis of *DACT1* mRNA levels normalized to *Gapdh* in BM2-TGC (**a**) and HPL1-TGC (**b**) cells stably transduced with *DACT1*-targeting shRNA (KD#1 and KD#2) or overexpression constructs. n = 4 technical repeats, Student's t-test. Data represents mean ± SEM. Student's t-test. **c, d**, Flow cytometry assessment of 7x-TCF-GFP Wnt reporter activity in BM2 (**c**) or HPL1 (**d**) cells with DACT1 knockdown or overexpression, n = 3 (c) and n = 4 (d) biological replicates. Student's t-test. Experiments were independently repeated >3 times (c) and 2 times (d). **e**, Immunofluorescence of total β-catenin in BM2 cells

with *DACT1* knockdown or overexpression with Wnt3a stimulation for 24 hours. Scale bars represent 50 μm. Representative of 2 independent replicates. **f**, Western blot of indicated proteins in BM2 cells with indicated DACT1-related constructs with Wnt3a or control media stimulation for 24 hours. Representative of 2 independent replicates. Numerical source data for **a-d** and uncropped blots for **f,** are provided.
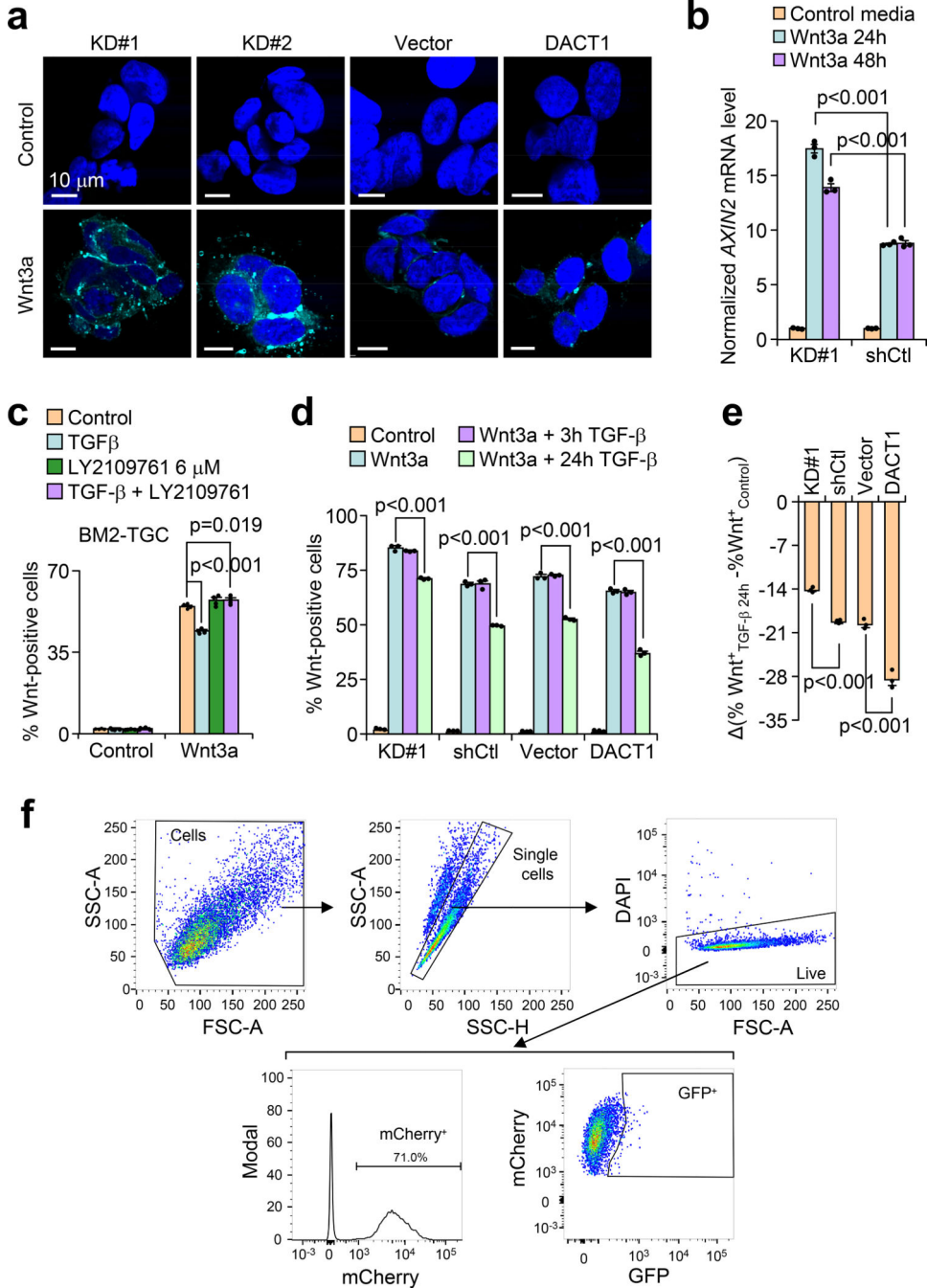
**Extended Data Fig. 3. TGF-β-induced *DACT1* suppresses Wnt signaling.**

a, Indirect immunofluorescence of β-catenin in the indicated *DACT1*-modified HPL1 cells with Wnt3a or control media for 24h. Mean pixel in intensities for Wnt3a-treated cells were measured at 9.041 (KD#1), 5.047 (KD#2), 1.562 (Vector), 1.356 (DACT1). Scale bars represent 10 μm. Representative of 2 independent replicates. **b**, qPCR analysis of *Axin2* mRNA in BM2 cells with stable DACT1 KD or control after treatment with Wnt3a for 24 or 48h. mRNA levels were normalized with *Gapdh* level and then *Axin2* levels were normalized to the respective control condition. n= 3 technical replicates, Student's t-test. Representative of 2 independent experiments. **c,** 7x-TCF-GFP Wnt reporter expressing BM2 cells were pre-treated for 24 hours with TGF-β and/or the TGF-β inhibitor LY2109761 followed by stimulation with Wnt3a and flow cytometry assessment of Wnt activation. n= 4 biological replicates. Student's t-test. **d**, **e**, BM2-TGC cells with the indicated modification of DACT1 were treated with Wnt3a or Wnt3a + TGF-β (3h or 24h pre-treatment) were quantified by flow cytometry. n= 4 biological replicates. Student's t-test. **f,** Gating strategy for flow cytometry quantification of 7TGC Wnt reporter activity. GFP[+] counts from GFP by mCherry panel corresponds to data in Figures 1e, 3c, 3f, 4d, 4e, Extended Figures 1m, 1n, 2c, 2d, 3c–e. Numerical source data for **b-e** are provided.
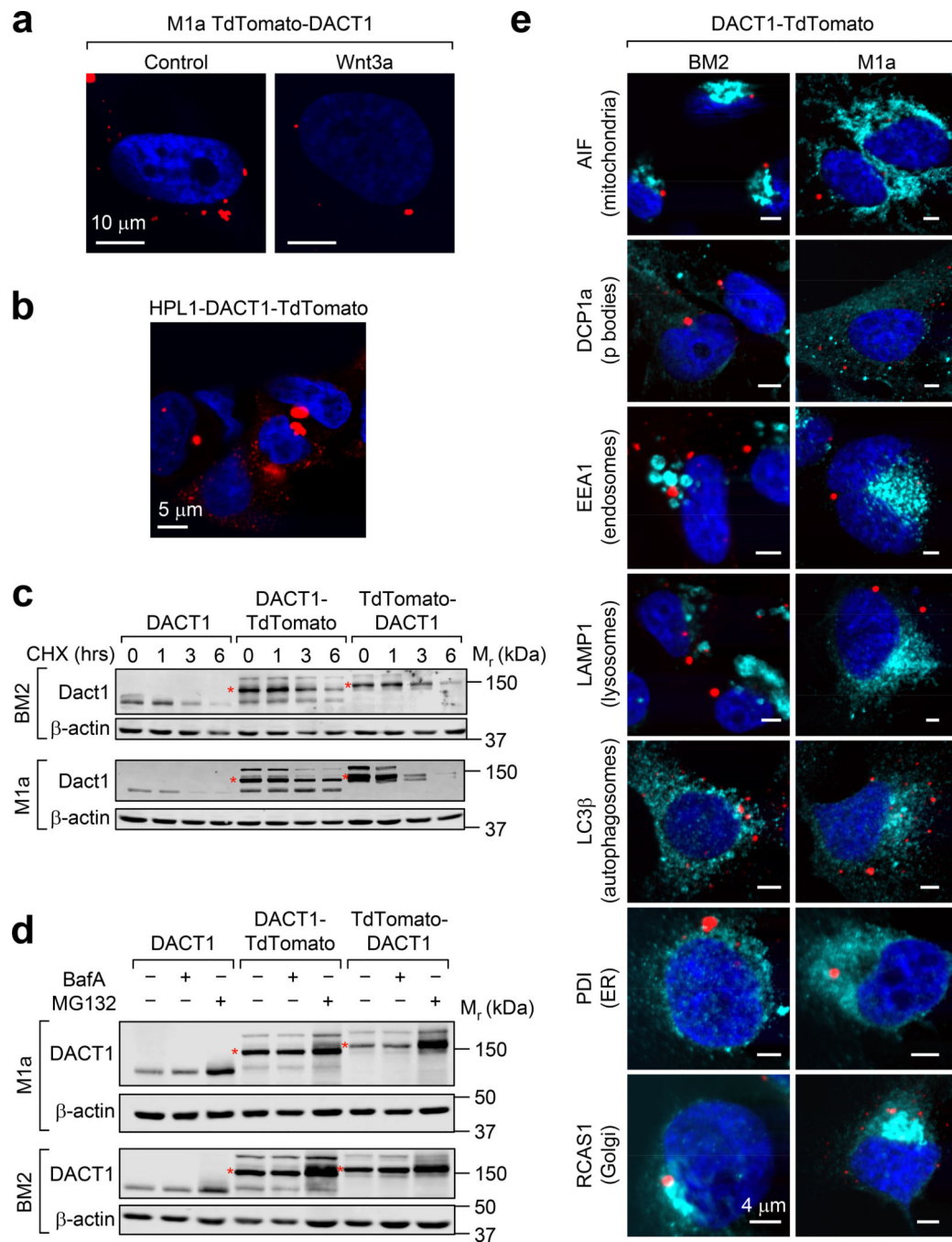
**Extended Data Fig. 4. DACT1 bodies are proteasomally degraded and do not co-localize with known organelles.**

a, DACT1-TdTomato fusion protein expression in M1a cells with or without 24h Wnt3a treatment. Scale bar represents 10 μm. Representative of n > 5 independent replicates. **b**, DACT1-TdTomato c-terminal fusions imaged in HPL1 cells. Scale bar represents 5 μm. Representative of n > 5 independent replicates. **c**, **d**, Western blot analysis of DACT1 wild-type and DACT1-TdTomato fusion protein expression in both M1a and BM2 cells after treatment with cycloheximide (50 μg/mL) at the indicated times (**c**) or either Bafilomycin A

(10 nM) or MG-132 (20 μM) for 12 h. (**d**). Images (**c, d**) representative of 3 independent experiments. * indicates expected molecular weight of fusion proteins. **e**, Representative images of DACT1-TdTomato fusions and the indicated organelle-associated proteins imaged by confocal sectioning. Scale bars represent 4 μm. Representative of 3 independent replicates. Uncropped blots for **c, d,** are provided.
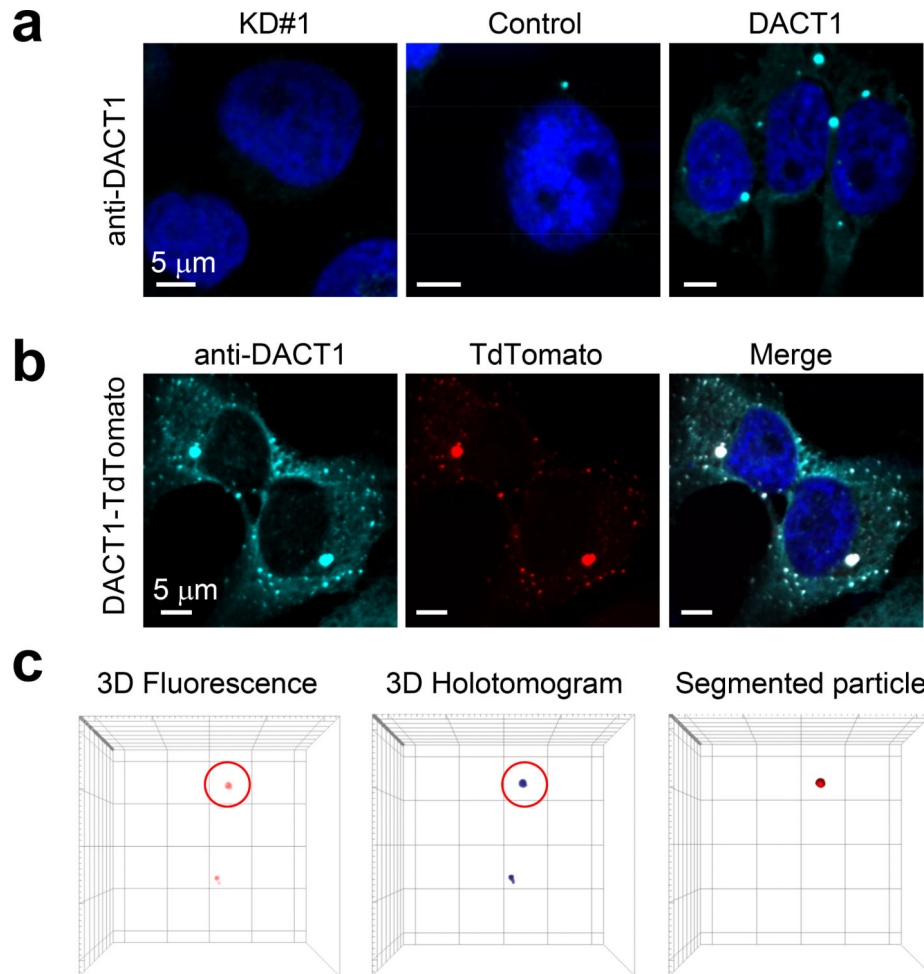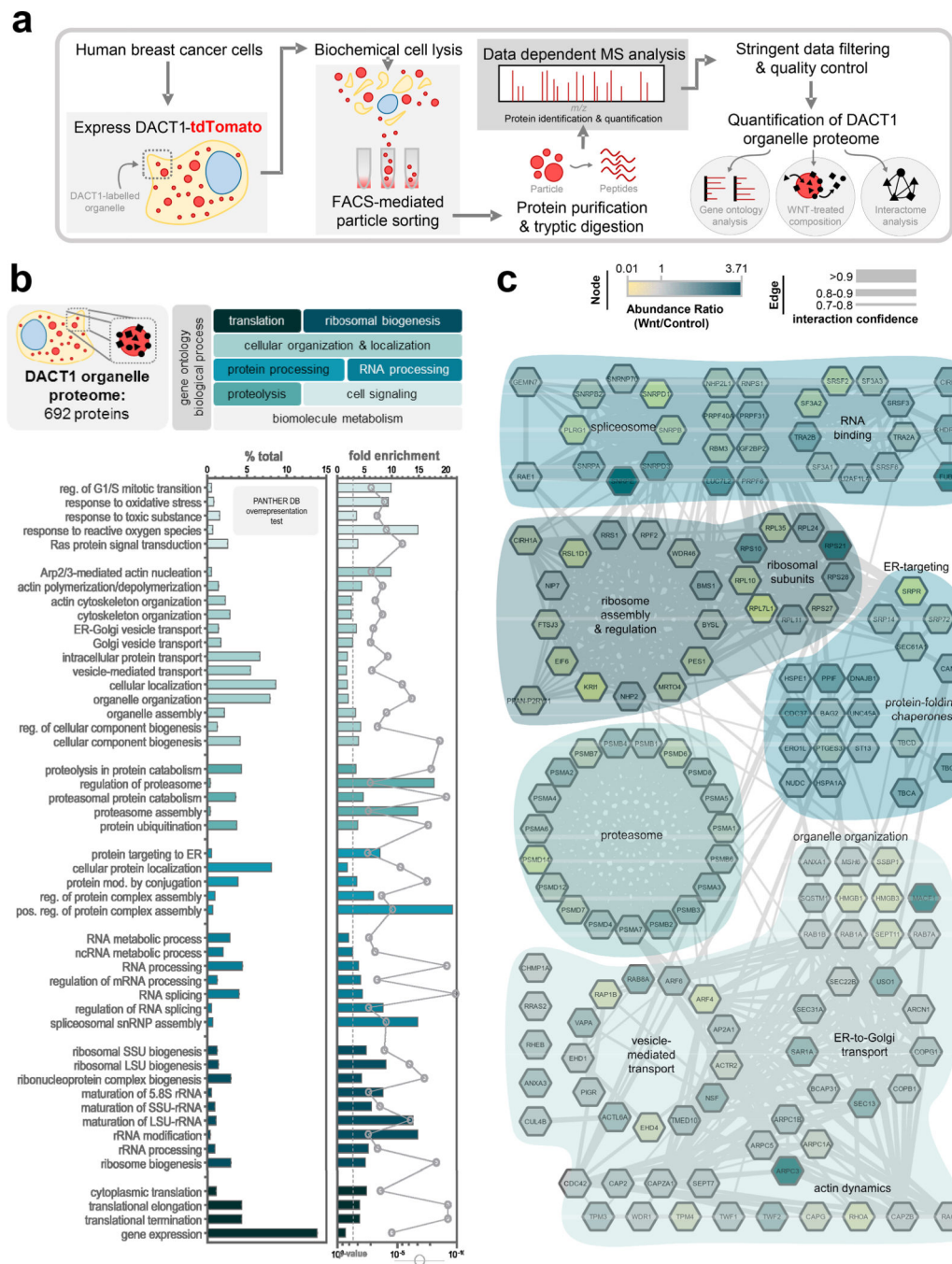

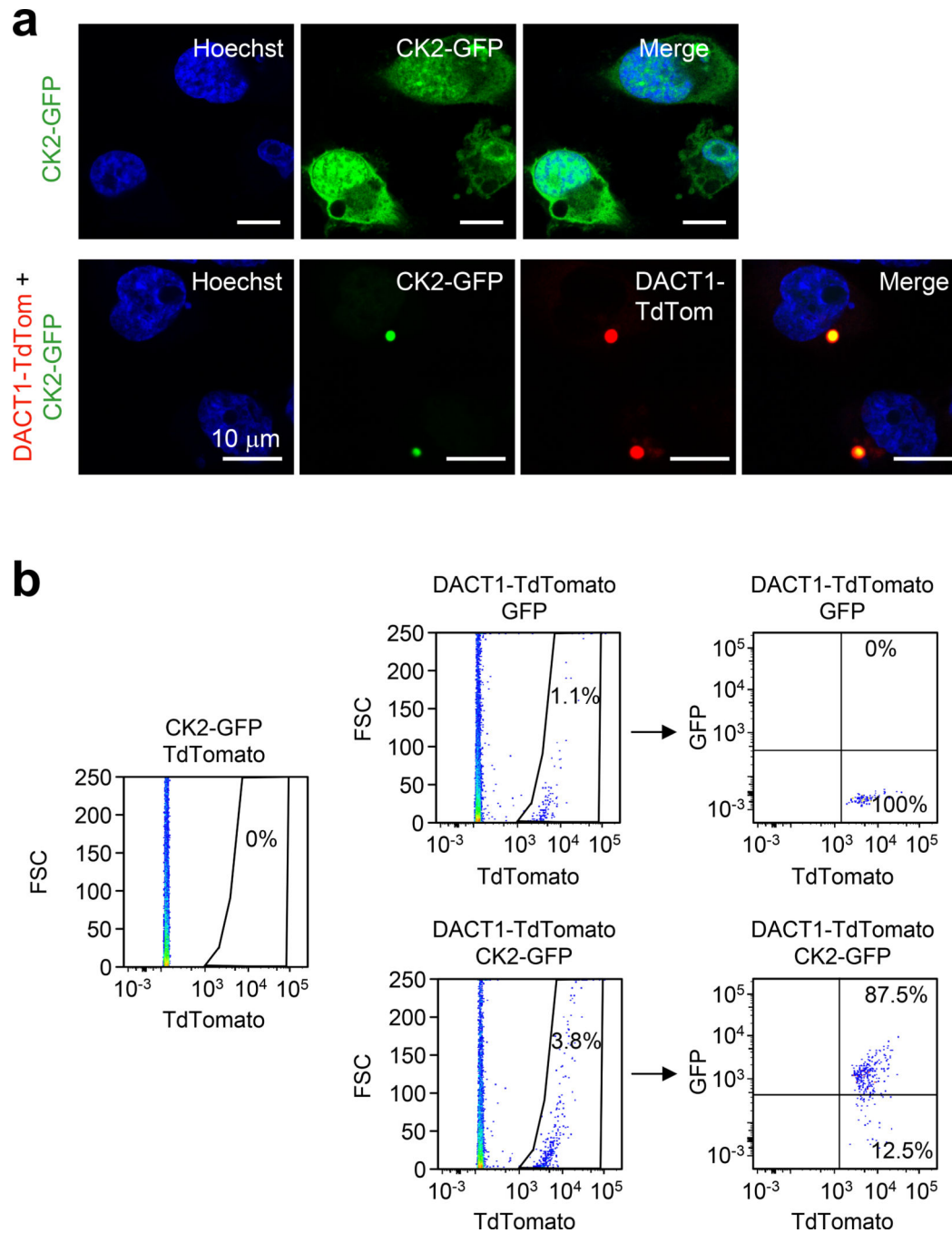**Extended Data Fig. 5. DACT1 particles show biomolecular condensation properties.**
a, **b**, DACT1 knockdown, control, overexpressing (**a**) or TdTomato c-terminal fusion cells (**b**) were probed with anti-DACT1 antibody followed by confocal imaging. Scale bars represent 5 μm. Images representative of 4 independent replicates. **c**, Holotomographic/epifluorescent particle sectioning analysis used to map refractive indices to 3D coordinates of TdTomato fluorescence.
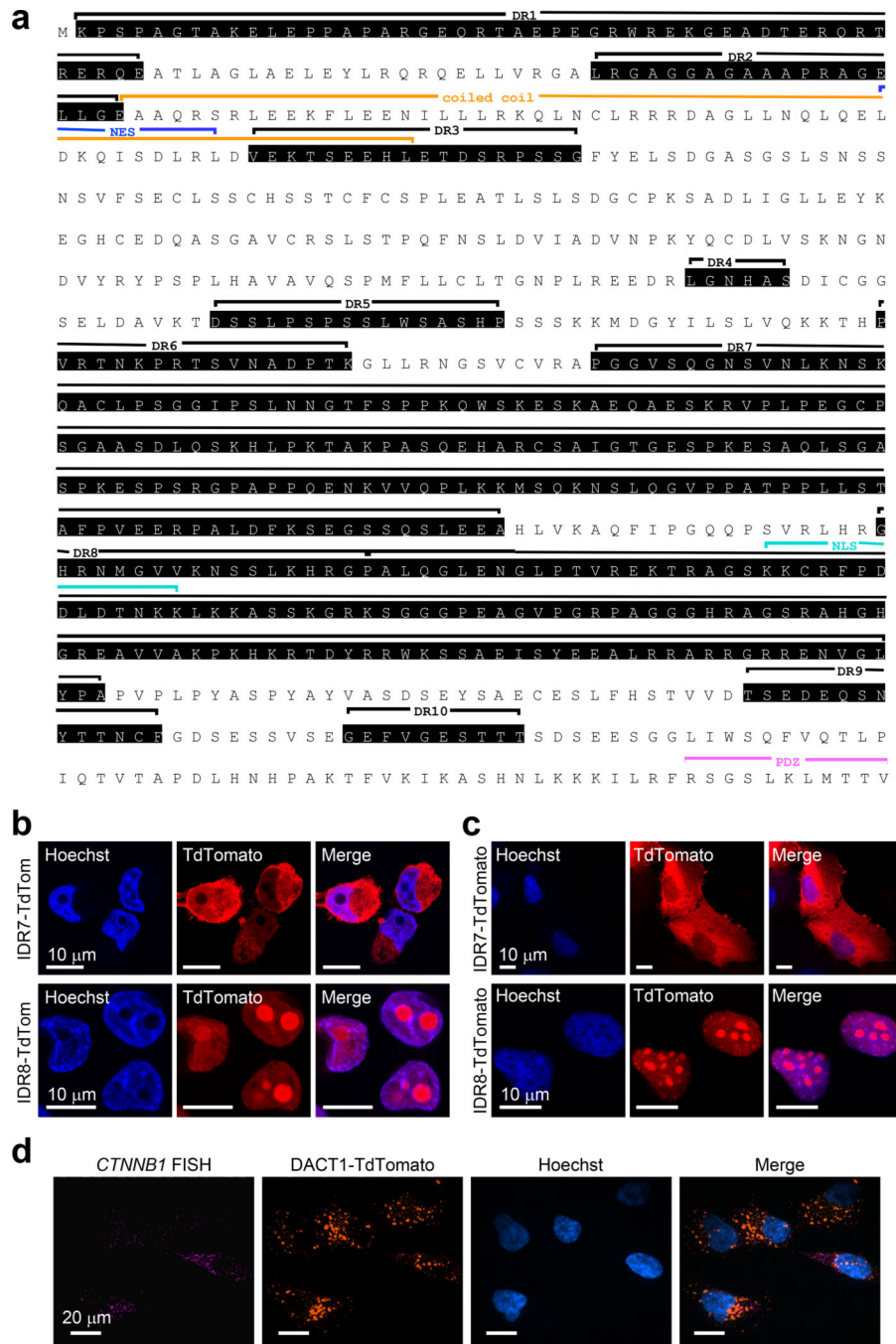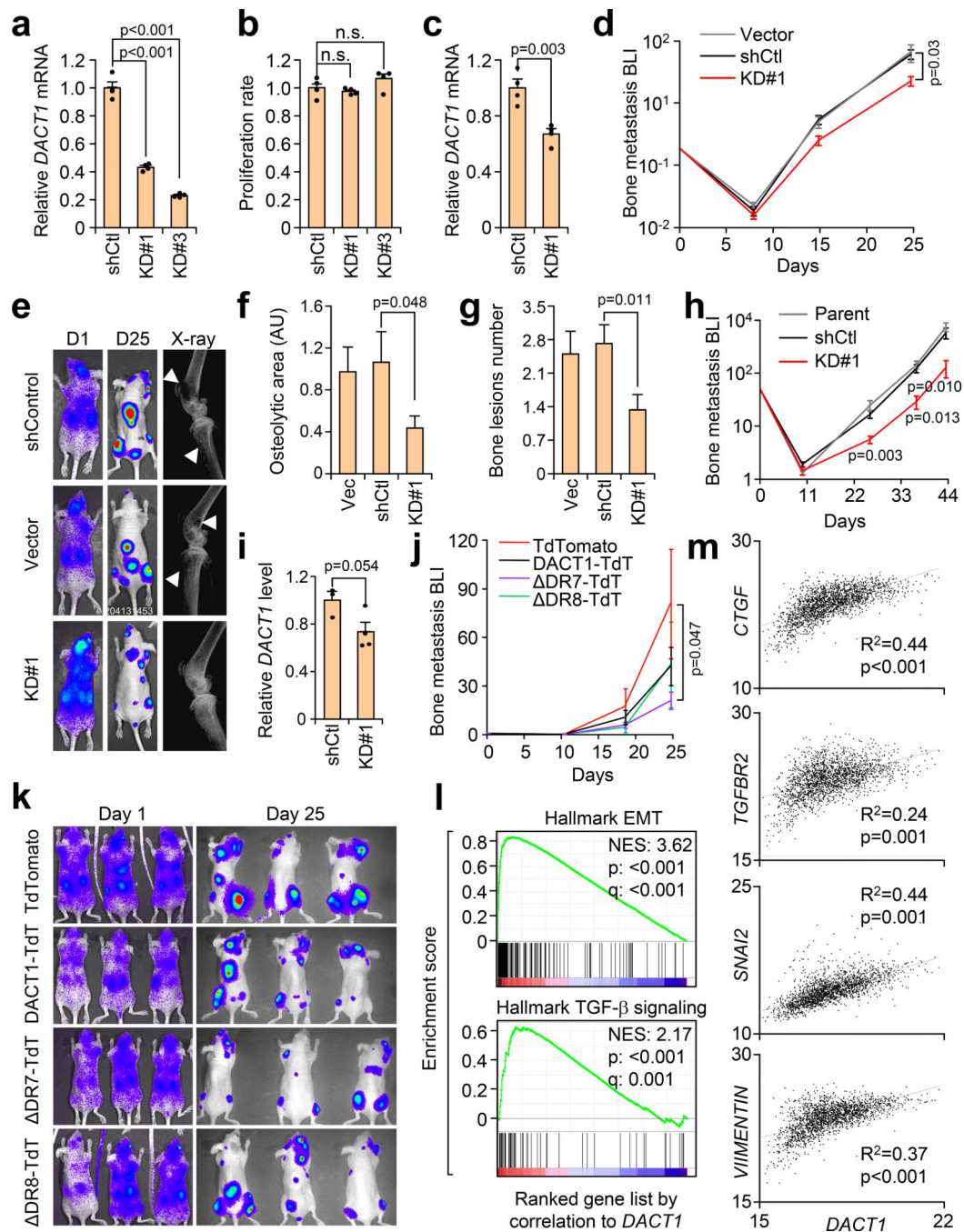
Extended Data Fig. 6. Deletion and hybrid mutant analysis of DACT1 protein localization.
a, Schematic of deletions made in the DACT1 amino acid sequence with predicted intrinsically disordered domains in black background and previously reported sequence motifs labeled in multiple colors. **b, c,** Confocal imaging of BM2 (c) and M1a (d) cells expressing DR7-TdTomato or DR8-TdTomato fusions labeled with Hoechst. Scale bars represent 10 µm. Representative of >3 independent replicates. **d**, Fluorescent *in situ* hybridization of RNA probes for *Ctnnb1* in BM2-hDACT1-TdTomato expressing cells. Scale bars represent 20 µm. Representative of 3 independent replicates.

Extended Data Fig. 7. Mass spectrometry analysis of DACT1 biomolecular condensates.
a, Isolation and analysis workflow for the characterization of DACT1-TdTomato particles. **b**, Proteins identified by mass spectrometry were analyzed by gene ontology using the Panther DB overrepresentation test with associated enrichment values and p-values. **c**, High stringency STRING analysis of identified proteins shows enriched protein interaction networks as related to biological processes. Protein background color correlates to enrichment ratio observed in Wnt3a-treated as compared to control-treated particles.

Extended Data Fig. 8. DACT1 sequesters cytoplasmic CK2 into condensates.
a, BM2 cells stably expressing CK2-GFP fusions alone or in combination with DACT1-TdTomato fusions were labeled with Hoechst and imaged via confocal microscopy. Scale bars represent 10 μm. Image representative of >5 independent replicates. **b,** M1a cells expressing constructs from (a) were subjected to the phase separation particle isolation protocol with the addition of GFP measurement. Experiment independently repeated 2 times.

Extended Data Fig. 9. DACT1 is essential for bone metastasis in models of breast and prostate cancer.

a, qRT-PCR analysis of *DACT1* mRNA levels normalized to *Gapdh* in the M1a cells stably transduced with DACT1-targeting shRNA or control shRNA. n = 4 technical repeats, representative data from 2 independent mRNA isolations and qRT-PCR experiments. Student's t-test. **b**, Proliferation rate over 24 hours was measured by WST-8 MTT assay and normalized to Control shRNA. n = 4 biological replicates, Student's t-test. **c**, qRT-PCR analysis of *DACT1* mRNA levels normalized to *Gapdh* in the BM2 cells stably transduced

with DACT1-targeting shRNA or control shRNA. n = 4 technical repeats, representative data from 2 independent mRNA isolations and qRT-PCR experiments. Student's t-test. **d**, BLI quantification of hind limb bone metastasis burden in mice injected with BM2 cells stably transduced with DACT1-targeting shRNA or control shRNA. Per-mouse signal was normalized to photon flux of the same mouse measured on Day 0 post-injection. n = 9 mice per group. Mann-Whitney U test. **e**, Representative bioluminescent and X-ray images from (**d**). **f, g,** The number (**f**) and area (**g**) of overt metastatic bone lesions were quantified per hindlimb per group with ImageJ. Mann-Whitney test. n = 18 (KD#1) and 14 (shCTL) hindlimbs per group. **h**, BLI quantification of hind limb bone metastasis burden in mice injected with DU145-ob2b cells stably transduced with DACT1-targeting shRNA or control shRNA. Per-mouse signal was normalized to photon flux of the same mouse measured on Day 0 post-injection. n= 9 mice per group. Mann-Whitney U test. **i**, qRT-PCR analysis of *DACT1* mRNA levels normalized to *Gapdh* in the DU145-ob2b cells stably transduced with DACT1-targeting shRNA or control shRNA. n = 4 technical repeats. Student's t-test. **j**, M1a cells stably expressing each DACT1 construct fused to TdTomato or TdTomato alone were inoculated via intracardiac injection and followed by bioluminescence. n = 9 mice per group. Experiment performed once. **k,** Representative images from (j). **l,** Correlation of *DACT1* expression values to indicated GOIs from the METABRIC dataset. **m,** Pearson correlation coefficients for each gene correlated to *DACT1* were ranked and GSEA analysis was performed to test the enrichment of the indicated gene sets in the Hallmark data set. Statistics by GSEA software. Data represents mean ± SEM. Student's t-test. Numerical source data for **a-d, f-j, m,** are provided.

Supplementary Material

Refer to Web version on PubMed Central for supplementary material.

Acknowledgments

References

1. Attisano L & Labbe E TGFbeta and Wnt pathway cross-talk. Cancer Metastasis Rev 23, 53–61 (2004). [PubMed: 15000149]

2. Glass DA 2nd et al. Canonical Wnt signaling in differentiated osteoblasts controls osteoclast differentiation. Dev Cell 8, 751–764 (2005). [PubMed: 15866165]

3. Retting KN, Song B, Yoon BS & Lyons KM BMP canonical Smad signaling through Smad1 and Smad5 is required for endochondral bone formation. Development 136, 1093–1104 (2009). [PubMed: 19224984]

4. Takaku K et al. Gastric and duodenal polyps in Smad4 (Dpc4) knockout mice. Cancer Res 59, 6113–6117 (1999). [PubMed: 10626800]

5. Fujita K & Janz S Attenuation of WNT signaling by DKK-1 and −2 regulates BMP2-induced osteoblast differentiation and expression of OPG, RANKL and M-CSF. Mol Cancer 6, 71 (2007). [PubMed: 17971207]

6. Winkler DG et al. Sclerostin inhibition of Wnt-3a-induced C3H10T1/2 cell differentiation is indirect and mediated by bone morphogenetic proteins. J Biol Chem 280, 2498–2502 (2005). [PubMed: 15545262]

7. Inkson CA et al. TGF-beta1 and WISP-1/CCN-4 can regulate each other's activity to cooperatively control osteoblast function. J Cell Biochem 104, 1865–1878 (2008). [PubMed: 18404666]

8. Bragado P et al. TGF-beta2 dictates disseminated tumour cell fate in target organs through TGF-beta-RIII and p38alpha/beta signalling. Nat Cell Biol 15, 1351–1361 (2013). [PubMed: 24161934]

9. Korpal M et al. Imaging transforming growth factor-β signaling dynamics and therapeutic response in breast cancer bone metastasis. Nature Medicine 15, 960–966 (2009).

10. Weilbaecher KN, Guise TA & McCauley LK Cancer to bone: a fatal attraction. Nature Reviews Cancer 11, 411–425 (2011). [PubMed: 21593787]

11. Esposito M, Guise T & Kang Y The Biology of Bone Metastasis. Cold Spring Harb Perspect Med 8 (2018).

12. Xu J et al. 14–3-3zeta turns TGF-beta's function from tumor suppressor to metastasis promoter in breast cancer by contextual changes of Smad partners from p53 to Gli2. Cancer Cell 27, 177–192 (2015). [PubMed: 25670079]

13. Sethi N, Dai X, Winter CG & Kang Y Tumor-Derived Jagged1 Promotes Osteolytic Bone Metastasis of Breast Cancer by Engaging Notch Signaling in Bone Cells. Cancer Cell 19, 192–205 (2011). [PubMed: 21295524]

14. Pfeilschifter J & Mundy GR Modulation of type beta transforming growth factor activity in bone cultures by osteotropic hormones. Proc Natl Acad Sci U S A 84, 2024–2028 (1987). [PubMed: 3494250]

15. Malladi S et al. Metastatic Latency and Immune Evasion through Autocrine Inhibition of WNT. Cell 165, 45–60 (2016). [PubMed: 27015306]

16. Zhuang X et al. Differential effects on lung and bone metastasis of breast cancer by Wnt signalling inhibitor DKK1. Nat Cell Biol 19, 1274–1285 (2017). [PubMed: 28892080]

17. Mariz K, Ingolf JB, Daniel H, Teresa NJ & Erich-Franz S The Wnt inhibitor dickkopf-1: a link between breast cancer and bone metastases. Clin Exp Metastasis 32, 857–866 (2015). [PubMed: 26420587]

18. Esposito M et al. Bone vascular niche E-selectin induces mesenchymal-epithelial transition and Wnt activation in cancer cells to promote bone metastasis. Nat Cell Biol 21, 627–639 (2019). [PubMed: 30988423]

19. Pronobis MI, Rusan NM & Peifer M A novel GSK3-regulated APC:Axin interaction regulates Wnt signaling by driving a catalytic cycle of efficient betacatenin destruction. Elife 4, e08022 (2015). [PubMed: 26393419]

20. Schwarz-Romond T, Merrifield C, Nichols BJ & Bienz M The Wnt signalling effector Dishevelled forms dynamic protein assemblies rather than stable associations with cytoplasmic vesicles. J Cell Sci 118, 5269–5277 (2005). [PubMed: 16263762]

21. Mitrea DM & Kriwacki RW Phase separation in biology; functional organization of a higher order. Cell Commun Signal 14, 1 (2016). [PubMed: 26727894]

22. Yang P et al. G3BP1 Is a Tunable Switch that Triggers Phase Separation to Assemble Stress Granules. Cell 181, 325–345 e328 (2020). [PubMed: 32302571]

23. Sanders DW et al. Competing Protein-RNA Interaction Networks Control Multiphase Intracellular Organization. Cell 181, 306–324 e328 (2020). [PubMed: 32302570]

24. Minn AJ et al. Genes that mediate breast cancer metastasis to lung. Nature 436, 518–524 (2005). [PubMed: 16049480]

25. Kang Y et al. A multigenic program mediating breast cancer metastasis to bone. Cancer Cell 3, 537–549 (2003). [PubMed: 12842083]

26. Forozan F et al. Molecular cytogenetic analysis of 11 new breast cancer cell lines. Br J Cancer 81, 1328–1334 (1999). [PubMed: 10604729]

27. Zheng H et al. Therapeutic Antibody Targeting Tumor- and Osteoblastic Niche-Derived Jagged1 Sensitizes Bone Metastasis to Chemotherapy. Cancer Cell 32, 731–747 e736 (2017). [PubMed: 29232552]

28. Shen M et al. Tinagl1 Suppresses Triple-Negative Breast Cancer Progression and Metastasis by Simultaneously Inhibiting Integrin/FAK and EGFR Signaling. Cancer Cell 35, 64–80 e67 (2019). [PubMed: 30612941]

29. Koinuma D et al. Chromatin immunoprecipitation on microarray analysis of Smad2/3 binding sites reveals roles of ETS1 and TFAP2A in transforming growth factor beta signaling. Mol Cell Biol 29, 172–186 (2009). [PubMed: 18955504]

30. Padua D et al. TGFbeta primes breast tumors for lung metastasis seeding through angiopoietin-like 4. Cell 133, 66–77 (2008). [PubMed: 18394990]

31. Kang Y, Chen CR & Massague J A self-enabling TGFbeta response coupled to stress signaling: Smad engages stress response factor ATF3 for Id1 repression in epithelial cells. Mol Cell 11, 915–926 (2003). [PubMed: 12718878]

32. Cheyette BN et al. Dapper, a Dishevelled-associated antagonist of beta-catenin and JNK signaling, is required for notochord formation. Dev Cell 2, 449–461 (2002). [PubMed: 11970895]

33. Gloy J, Hikasa H & Sokol SY Frodo interacts with Dishevelled to transduce Wnt signals. Nat Cell Biol 4, 351–357 (2002). [PubMed: 11941372]

34. Waxman JS, Hocking AM, Stoick CL & Moon RT Zebrafish Dapper1 and Dapper2 play distinct roles in Wnt-mediated developmental processes. Development 131, 5909–5921 (2004). [PubMed: 15539487]

35. Hikasa H & Sokol SY The involvement of Frodo in TCF-dependent signaling and neural tissue development. Development 131, 4725–4734 (2004). [PubMed: 15329348]

36. Park JI et al. Frodo links Dishevelled to the p120-catenin/Kaiso pathway: distinct catenin subfamilies promote Wnt signals. Dev Cell 11, 683–695 (2006). [PubMed: 17084360]

37. Zhang L, Gao X, Wen J, Ning Y & Chen YG Dapper 1 antagonizes Wnt signaling by promoting dishevelled degradation. J Biol Chem 281, 8607–8612 (2006). [PubMed: 16446366]

38. Gao X et al. Dapper1 is a nucleocytoplasmic shuttling protein that negatively modulates Wnt signaling in the nucleus. J Biol Chem 283, 35679–35688 (2008). [PubMed: 18936100]

39. Chen H et al. Protein kinase A-mediated 14–3-3 association impedes human Dapper1 to promote dishevelled degradation. J Biol Chem 286, 14870–14880 (2011). [PubMed: 21262972]

40. Ma B et al. Dapper1 promotes autophagy by enhancing the Beclin1-Vps34-Atg14L complex formation. Cell Res 24, 912–924 (2014). [PubMed: 24980960]

41. Huang Y, Wang P, Chen H, Ding Y & Chen YG Myc-interacting zinc-finger protein 1 positively regulates Wnt signalling by protecting Dishevelled from Dapper1-mediated degradation. Biochem J 466, 499–509 (2015). [PubMed: 25558878]

42. Kivimae S, Yang XY & Cheyette BN All Dact (Dapper/Frodo) scaffold proteins dimerize and exhibit conserved interactions with Vangl, Dvl, and serine/threonine kinases. BMC Biochem 12, 33 (2011). [PubMed: 21718540]

43. Fuerer C & Nusse R Lentiviral vectors to probe and manipulate the Wnt signaling pathway. PLoS One 5, e9370 (2010). [PubMed: 20186325]

44. Biechele TL, Adams AM & Moon RT Transcription-based reporters of Wnt/beta-catenin signaling. Cold Spring Harbor protocols 2009, pdb prot5223 (2009). [PubMed: 20147181]

45. Ma B et al. The Wnt Signaling Antagonist Dapper1 Accelerates Dishevelled2 Degradation via Promoting Its Ubiquitination and Aggregate-induced Autophagy. J Biol Chem 290, 12346–12354 (2015). [PubMed: 25825496]

46. Voros J The density and refractive index of adsorbing protein layers. Biophys J 87, 553–561 (2004). [PubMed: 15240488]

47. Banani SF, Lee HO, Hyman AA & Rosen MK Biomolecular condensates: organizers of cellular biochemistry. Nat Rev Mol Cell Biol 18, 285–298 (2017). [PubMed: 28225081]

48. Weber SC & Brangwynne CP Getting RNA and protein in phase. Cell 149, 1188–1191 (2012). [PubMed: 22682242]

49. Schaefer KN & Peifer M Wnt/Beta-Catenin Signaling Regulation and a Role for Biomolecular Condensates. Dev Cell 48, 429–444 (2019). [PubMed: 30782412]

50. Feric M et al. Coexisting Liquid Phases Underlie Nucleolar Subcompartments. Cell 165, 1686–1697 (2016). [PubMed: 27212236]

51. Woodruff JB, Hyman AA & Boke E Organization and Function of Non-dynamic Biomolecular Condensates. Trends in biochemical sciences 43, 81–94 (2018). [PubMed: 29258725]

52. Bracha D et al. Mapping Local and Global Liquid Phase Behavior in Living Cells Using Photo-Oligomerizable Seeds. Cell 175, 1467–1480 e1413 (2018). [PubMed: 30500534]

53. Hubstenberger A et al. P-Body Purification Reveals the Condensation of Repressed mRNA Regulons. Mol Cell 68, 144–157 e145 (2017). [PubMed: 28965817]

54. Gao Y & Wang HY Casein kinase 2 Is activated and essential for Wnt/beta-catenin signaling. J Biol Chem 281, 18394–18400 (2006). [PubMed: 16672224]

55. Vinayagam A et al. A directed protein interaction network for investigating intracellular signal transduction. Sci Signal 4, rs8 (2011). [PubMed: 21900206]

56. Curtis C et al. The genomic and transcriptomic architecture of 2,000 breast tumours reveals novel subgroups. Nature 486, 346–352 (2012). [PubMed: 22522925]

57. Bos PD et al. Genes that mediate breast cancer metastasis to the brain. Nature 459, 1005–1009 (2009). [PubMed: 19421193]

58. Bracha D et al. Mapping Local and Global Liquid Phase Behavior in Living Cells Using Photo-Oligomerizable Seeds. Cell 176, 407 (2019). [PubMed: 30633909]

59. Webb BD et al. Heterozygous Pathogenic Variant in DACT1 Causes an Autosomal-Dominant Syndrome with Features Overlapping Townes-Brocks Syndrome. Hum Mutat 38, 373–377 (2017). [PubMed: 28054444]
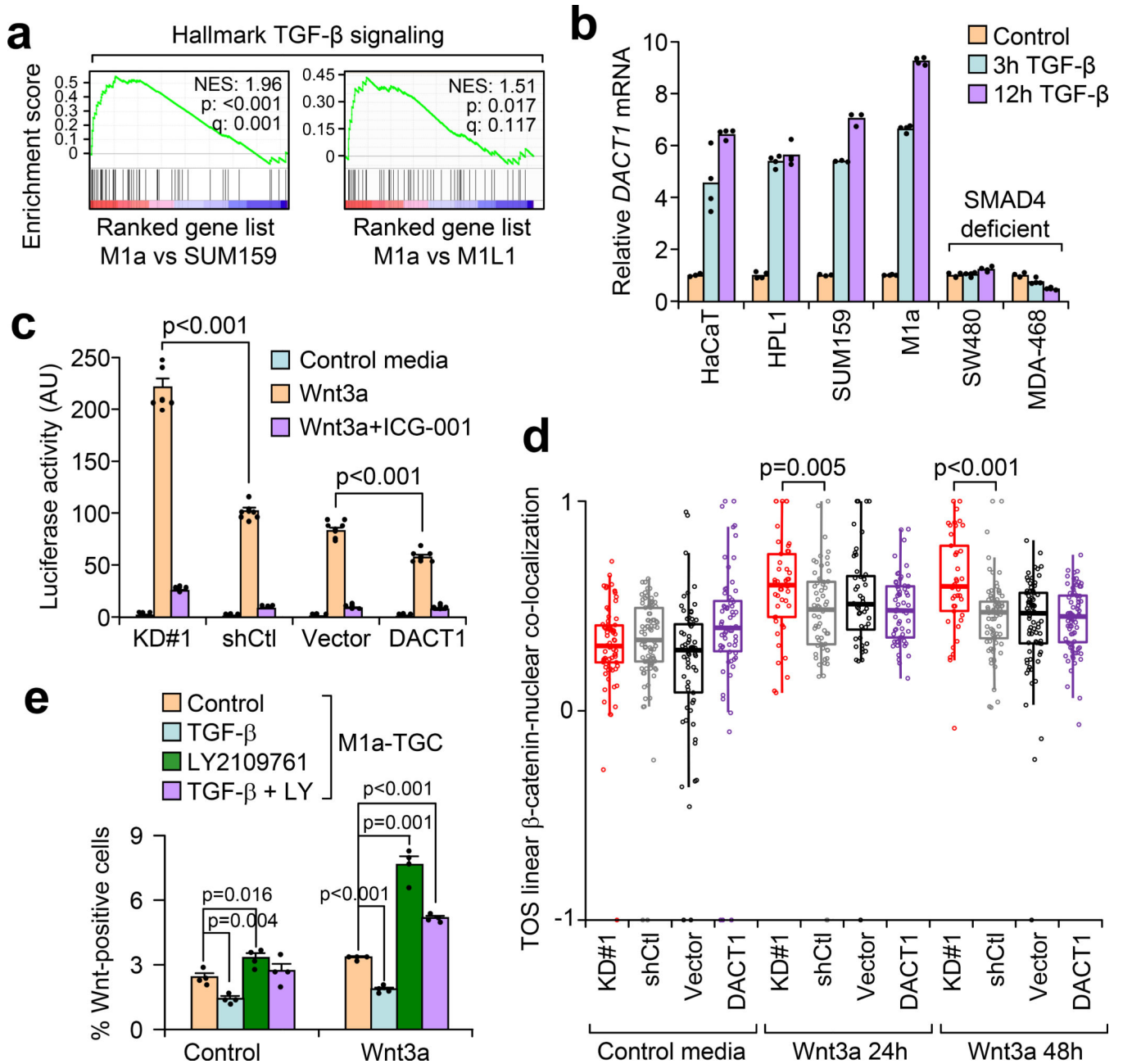
Fig. 1. TGF-β transcriptionally induces *DACT1* to repress Wnt signaling.
a, Gene set enrichment analysis of microarray data comparing gene expression of the bone-metastatic M1a derivative to either the parental SUM159 cell line or the M1L1 lung metastatic derivative tested against the Hallmark G1 data set (Broad Institute 2019). Statistics by GSEA software. **b**, qRT-PCR analysis of *DACT1* mRNA expression following the indicated duration of treatment with 200 pM TGF-β in various cancer and normal cell lines. *DACT1* levels were normalized to *Gapdh*. n = 3 technical replicates. Representative of 2 independent experiments. **c,** BM2 cells engineered with a 12x-TCF firefly luciferase reporter (12x-TCF-ffLUC) and stable knockdown or overexpression of *DACT1* were treated with control media, Wnt3a media, or Wnt3a media plus ICG-001 (25 μM) for 20h and then

luciferase activity was measured. n= 6 biological replicates per sample. Student's t-test. Experiment independently repeated >3 times. **d,** BM2 cells with stable *DACT1* knockdown, shControl (shCtl), vector control or ectopic expression were treated with control media or Wnt3a at 24 and 48 hours. Cells were fixed and immuno-labeled with anti-total β-catenin plus Hoechst (sample images in Extended Data Fig. 2e). The TOS linear algorithm was used to assess correlation of β-catenin and Hoechst colocalization. Statistics by EZCoLoc software. n = 75, 70, 89 (Vector); 103, 71, 88 (shCtl); 75, 70, 88 (DACT1); 79, 55, 50 (KD#1) cells analyzed across four biological replicates. Box plots represent median value with upper and lower quartiles while whiskers represent 1.5x interquartile range. Student's T-test, two-sided, no adjustments for multiple comparisons. **e**, 7x-TCF-GFP Wnt reporter expressing M1a cells were pre-treated for 24 hours with TGF-β and/or the TGF-β inhibitor LY2109761 (6 μM) followed by stimulation with Wnt3a and flow cytometry assessment of Wnt activation. n= 4 biological replicates. Student's t-test. Data represents mean ± SEM. Numerical source data for **b-e** are provided.
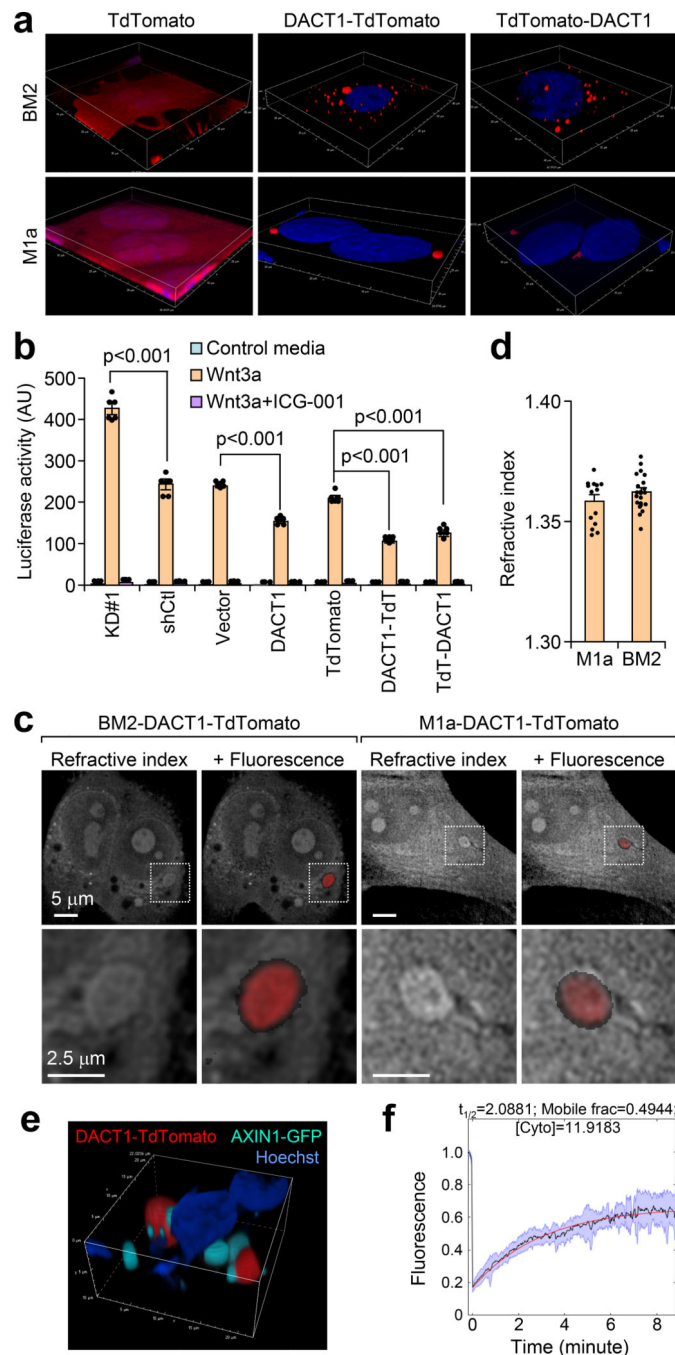
Fig. 2. Formation of DACT1-associated biomolecular condensates.

a, Lentiviruses expressing TdTomato or DACT1-TdTomato (C-terminal and N-Terminal) fusions were stably transduced into M1a and BM2 cells followed by confocal z-stacking of fixed cells counterstained with Hoechst. Images presented as 3-dimensional rendering of individual z-stacks. **b**, 12x-TCF-ffLUC Wnt reporter expressing BM2 cells were genetically modified to express the indicated *DACT1* knockdown, control or overexpression construct. The cell lines were treated with control media, Wnt3a or Wnt3a plus ICG-001 (25 μM) for 20h and Wnt activation was quantified by luciferase activity. n = 4 biological replicates,

experiment independently repeated 3 times. Student's t-test. **c**, Holotomographic images coupled to epifluorescence obtained by Tomocube™ imaging system shows refractive index as grayscale and fluorescence in red pseudocolor. Areas highlighted by dotted squares in the upper panels were enlarged in the lower panels. **d**, Quantification of refractive index in regions of red fluorescence in n = 22 (BM2) and 14 (M1a) distinct cells imaged across 3 independent experiments. Imaging sectioning analysis demonstrated in Extended Data Fig. 5c. **e**, Confocal z-stack of Axin1-GFP and DACT1-TdTomato transfectants in 293T cells. **f**, FRAP analysis of DACT1-TdTomato biomolecular condensate in BM2 cells. Data represents mean ± SEM. Numerical source data for **b, d,** are provided.
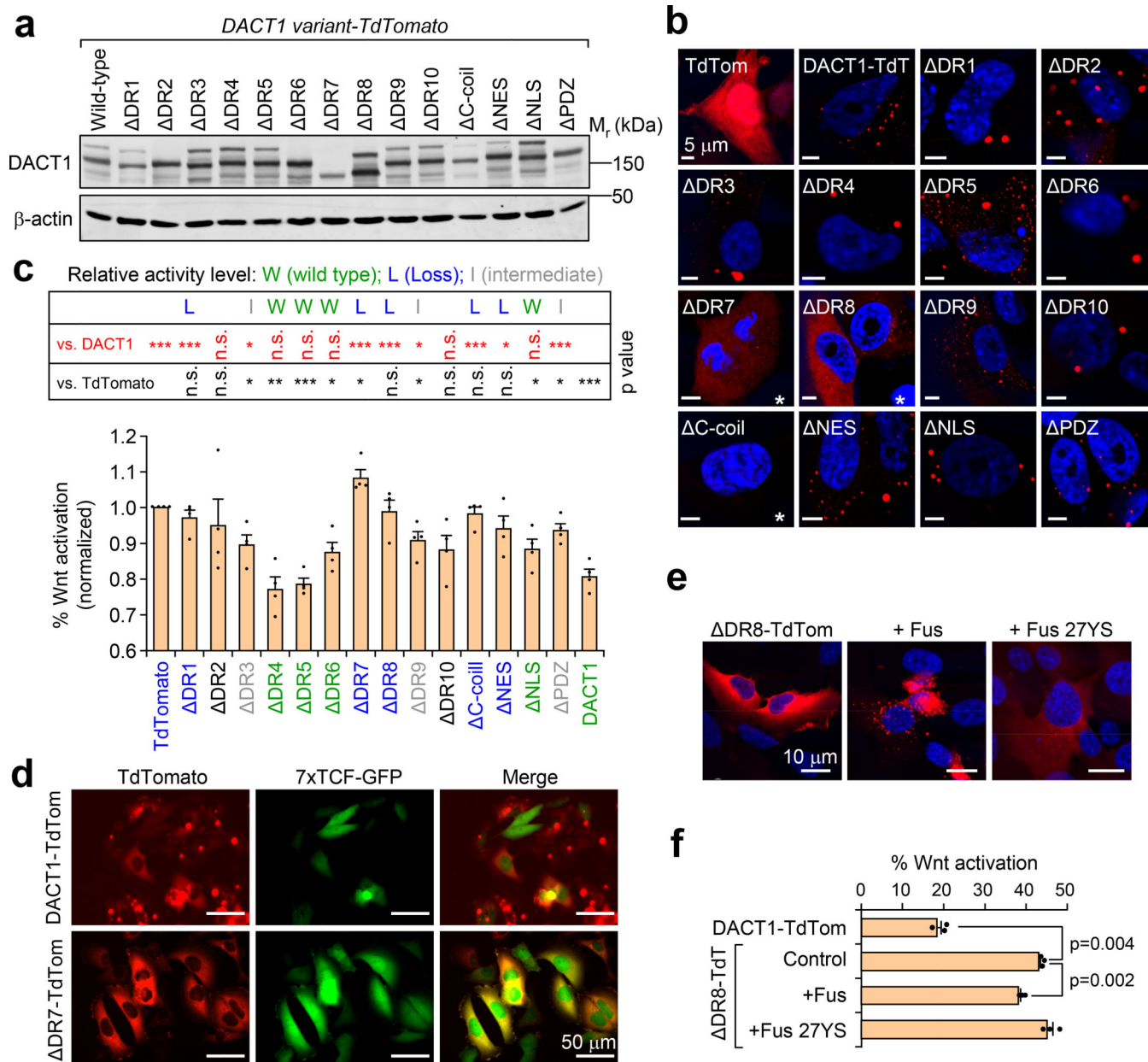
Fig. 3. DACT1 intrinsically disordered domains drive phase separation and Wnt suppression.
a, Western blot analysis of DACT1 mutants fused to TdTomato at the c-terminal region stably expressed in the BM2–7xTCF-GFP cell line. Deleted region 7 includes the antibody epitope recognition site and therefore ΔDR7 cannot be detected by western blot. Representative of 3 independent replicates. **b**, Confocal imaging of DACT1-TdTomato mutants stably expressed in the M1a cell line. Images representative of >3 independent experiments across both the BM2 and M1a cell lines. Scale bars represent 5 μm. Images marked with * have a lowered LUT threshold to adequately visualize signal. **c**, Wnt activation analysis of DACT1-TdTomato mutants expressed in the BM2–7xTCF-GFP cell line treated with Wnt3a for 24h. n=4 biological replicates pooled from 4 independent experiments. Student's t-test compares to TdTomato-only cells as the upper bound and

DACT1 wild-type as the lower bound. Wild-type (W) indicates Wnt repression was statistically insignificant compared to unmodified DACT1-TdTomato, while Loss (L) indicates insignificance compared only to TdTomato control. Intermediate (I) denotes significance compared to both controls. * p< 0.05, ** p<0.01, *** p<0.005 with exact p values in Source Data. Data represents mean ± SEM. **d**, DACT1-TdTomato or DACT1 DR7-TdTomato constructs were stably expressed in BM2–7xTCF-GFP cells and were treated with Wnt3a for 24h followed by live-cell confocal imaging. Images shown are representative of >3 independent experiments. **e**, Confocal imaging of DACT1-TdTomato c-terminal fusions in M1a cells with disordered region #8 deleted (DR8) compared with those same constructs with wild-type Fus or mutated Y > S 27x Fus mutants. Scale bars represent 10 μm. **f**, Constructs from (**e**) were introduced into BM2–7x-TCF-GFP Wnt reporter cells and the Wnt activation assay was performed. n= 3 biological replicates, independently repeated 2 times. Student's t-test. Numerical source data for **c, f,** and uncropped blots for **a,** are provided.
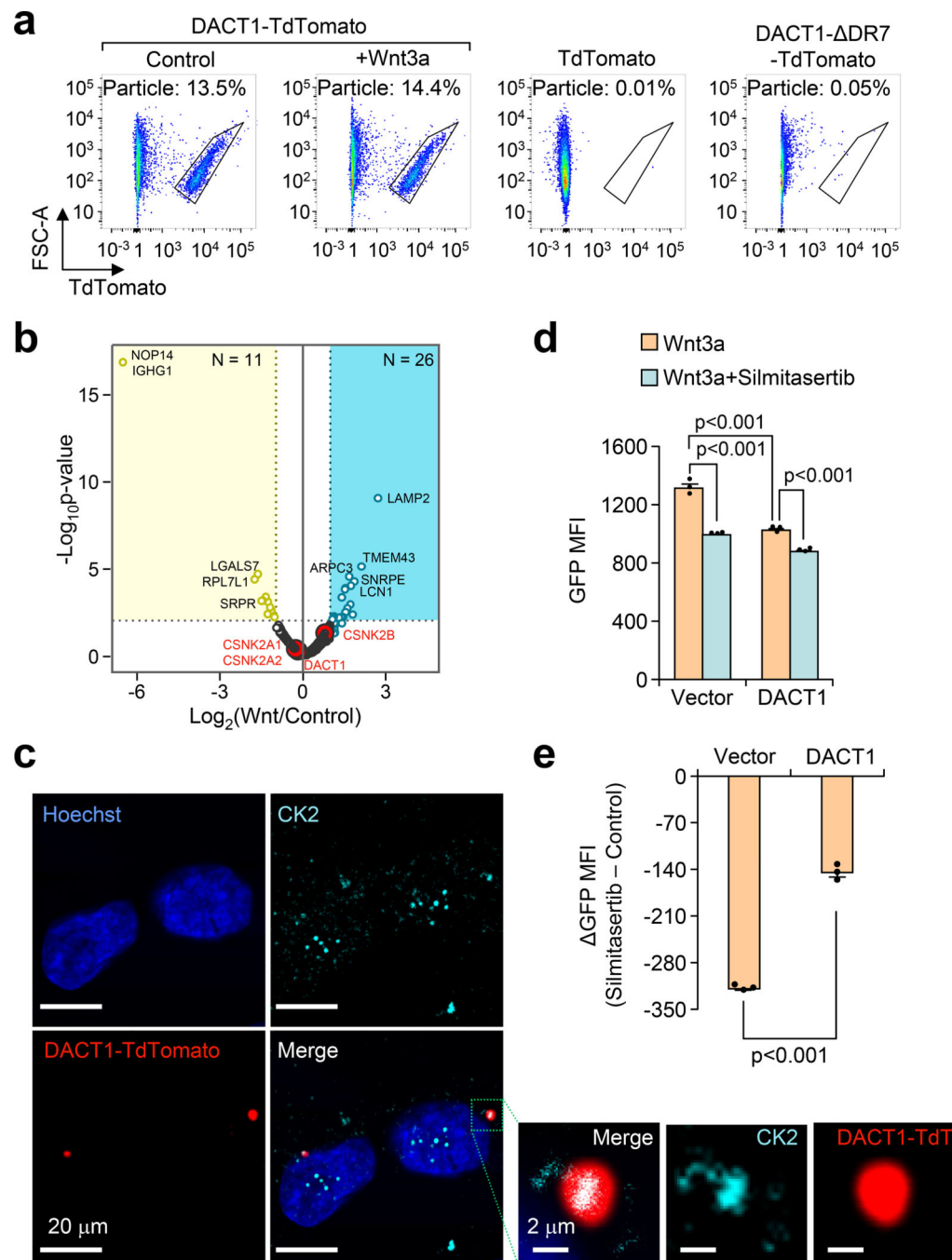
Fig. 4. Isolation and characterization of DACT1 biomolecular condensates.

a, BM2 cells stably expressing hDACT1-TdTomato fusions were treated with control or Wnt3A media for 24h. Cells were sonicated in PBS followed by addition of 1% Triton X-100, 0.5% Sodium Deoxycholate, Hoechst (10 μg/ml). Particulate suspensions were analyzed and sorted via a modified FACS protocol using TdTomato only and DACT1-TdTomato- DR7 mutant particulate suspensions as negative gating controls. Experiment was analyzed on a BD LSRII >3 times and particles were sorted on a BD FACSAria Fusion and analyzed via mass spectrometry. n = 4 independent isolations with similar results. **b**,

Volcano plot of proteins enriched in the Wnt3a vs. control-treated conditions. Only two proteins (NOP14, IGHG1) were detected only in the control condition and not the Wnt3a condition. n = 3 independent isolations and mass spectrometry analyses per condition. **c**, Confocal imaging of indirect immunofluorescent staining for CK2 in BM2-hDACT1-TdTomato cells. Co-localization of DACT1-TdTomato with cytoplasmic CK2 was highlighted in close-up images in the area marked by a dotted line box. Scale bars represent 20 μm. Magnified view scale bars represent 2 μm. Images representative of 2 independent experiments. **d**, BM2-TGC cells expressing either vector or *DACT1* were treated with Wnt3a +/− Silmitasertib at 5 μM for 24h. **e,** Median fluorescence intensities from **(c)** of the Wnt3a treated condition (n = 3 biological replicates) were averaged and subtracted from individual MFI values for silmitasertib-treated cells (n= 3 biological replicates). Student's t-test. Experiment representative of 3 independent replicates. Data represents mean ± SEM. Numerical source data for **b, d, e** are provided.
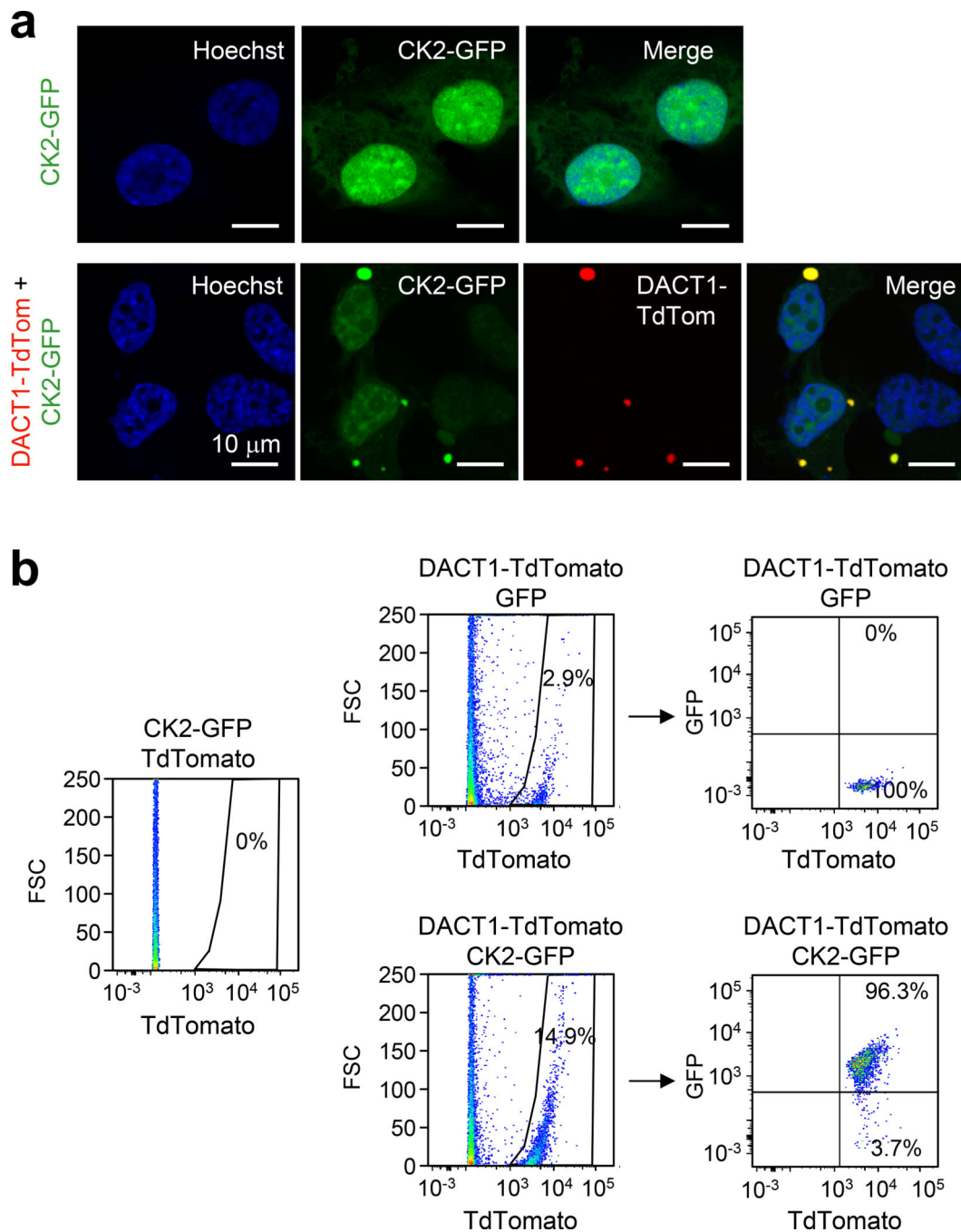
Fig. 5. DACT1 sequesters cytoplasmic CK2 into condensates.
a, M1a cells stably expressing CK2α-GFP fusions alone or in combination with DACT1-TdTomato fusions were labeled with Hoechst and imaged via confocal microscopy. Scale bars represent 10 μm. Image representative of 3 independent replicates. **b,** BM2 cells expressing constructs from (a) were subjected to the phase separation particle isolation protocol followed by FACS analysis showing enriched localization of CK2α-GFP in DACT1-TdTomato containing particles. Experiment independently repeated 2 times.
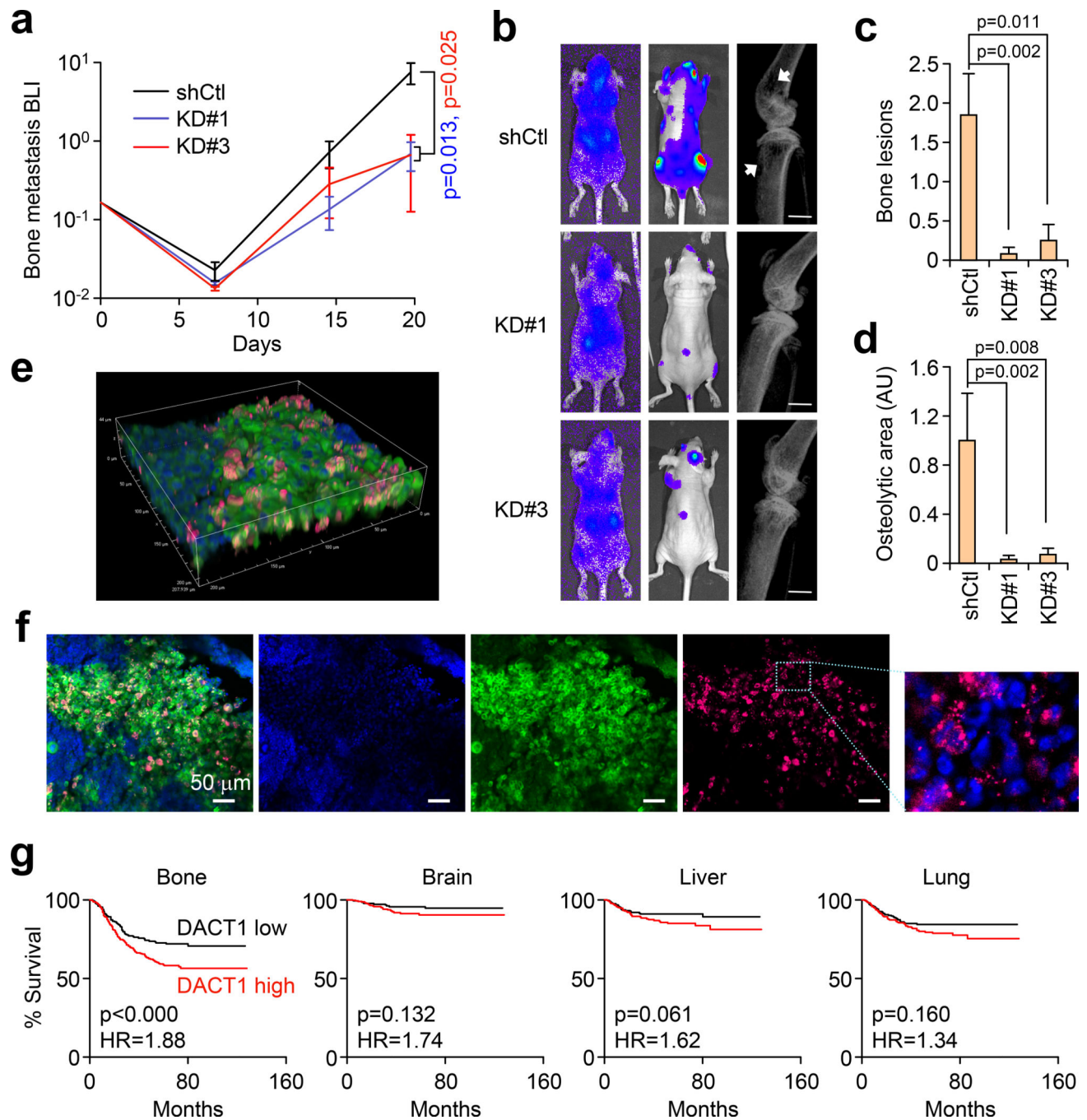
Fig. 6. DACT1 is necessary for bone metastasis growth.

a, Bioluminescent monitoring of mice injected with control or DACT1-knockdown M1a cells. BLI signals from bone metastases in the hind limbs was quantified. Per-mouse signal was normalized to photon flux of the same mouse measured on Day 0 post-injection. Statistics by repeated measures ANOVA comparing each KD cell line to the control cells expressing scrambled control shRNA (shCtrl). Same statistical patterns held for Mann-Whitney U test comparing normalized flux at day of final measurement. n = 8 (shCtl) 7 (KD#1) 6 (KD#3) mice per group. Experiment independently repeated 3 times with identical

trends. **b**, Representative BLI images immediately following injection and at the final day of measurement as well as sample *ex vivo* X-ray images. Scale bar represents 1.25 mm. **c**, **d**, The number (**c**) and area (**d**) of overt metastatic bone lesions were quantified per hind limb per group with ImageJ. Mann-Whitney test. n = 14 (shCtl), 13 (KD#1) and 12 (KD#2) hind limbs per group. **e**, **f**, Confocal z-stacks of *ex vivo* bone sections from nu/nu mice injected with GFP and DACT1-TdTomato expressing BM2 cells. Scale bars represent 50 μm. Image representative of >4 independent biological replicates. **g**, Kaplan-Meier survival curves from EMC-MSK dataset stratifying patients by median expression of *DACT1*. Hazard ratio and p-value by Cox's proportional hazards model. Data represents mean ± SEM. Numerical source data for **a, c, d, g,** are provided.